REPORT NO. FRA/ORD-80/45 PB

DEVELOPMENT OF A PROTOTYPE EMAT SYSTEM FOR INSPECTION OF RAILS

SEPTEMBER 1980
FINAL REPORT

Prepared for
U.S. DEPARTMENT OF TRANSPORTATION
FEDERAL RAILROAD ADMINISTRATION
Office of Research and Development
Washington, D.C. 20590

NOTICE

This document is disseminated under the sponsorship of the Department of Transportation in the interest of information exchange. The United States Government assumes no liability for its contents or use thereof.

NOTICE

The United States Government does not endorse products or manufacturers. Trade or manufacturers' names appear herein solely because they are considered essential to the object of this report.

Technical Report Documentation Page

1. Report No.	2. Government Accession No.	3. Recipient's Catalog No.
FRA/ORD-80/45		

4. Title and Subtitle	5. Report Date
Development of a Prototype EMAT System for Inspection of Rails	September 1980
	6. Performing Organization Code
	8. Performing Organization Report No.
7. Author(s)	
G. Alers, D. McLauchlan, H. Maiseri, and R. Lee	
9. Performing Organization Name and Address	10. Work Unit No. (TRAIS)
Rockwell International Albuquerque Development Laboratory 2340 Alamo S.E. Albuquerque, New Mexico 87106	11. Contract or Grant No. DOT-FR-9143
	13. Type of Report and Period Covered Final Report October 1979-March 1980
12. Sponsoring Agency Name and Address	14. Sponsoring Agency Code
U.S. Department of Transportation Federal Railroad Administration 400 Seventh Street, S.W. Washington, D.C. 20590	DOT/FRA

15. Supplementary Notes

16. Abstract

This is the Final Report of the First Phase of an investigation of the application of Electromagnetic Acoustic Transducers (EMAT's) to detect flaws in railroad rails. EMAT's generate ultrasonic beams in rails and receive return signals without surface contact and without liquid couplant. This work used samples of flawed rails and laboratory EMAT equipment to verify that EMAT technology can detect critical rail flaws. Sperry Rail Service assisted in defining operating requirements for an operational inspection system. A preliminary determination of EMAT operating parameters for optimum flaw detection was made.

This work demonstrated that virtually all of the critical rail flaws can be detected in the laboratory by EMAT's with a sensitivity comparable to that obtained with conventional piezoelectric transducers.

17. Key Words	18. Distribution Statement
Electromagnetic Acoustic Transducer (EMAT), rail flaw, inspection methods	Document is available to the public through the National Technical Information Service, Springfield, Virginia 22161

19. Security Classif. (of this report)	20. Security Classif. (of this page)	21. No. of Pages	22. Price
Unclassified	Unclassified	77	

Form DOT F 1700.7 (8-72) Reproduction of completed page authorized

METRIC CONVERSION FACTORS

Approximate Conversions to Metric Measures

Symbol	When You Know	Multiply by	To Find	Symbol
		LENGTH		
in	inches	*2.5	centimeters	cm
ft	feet	30	centimeters	cm
yd	yards	0.9	meters	m
mi	miles	1.6	kilometers	km
		AREA		
in^2	square inches	6.5	square centimeters	cm^2
ft^2	square feet	0.09	square meters	m^2
yd^2	square yards	0.8	square meters	m^2
mi^2	square miles	2.6	square kilometers	km^2
	acres	0.4	hectares	ha
		MASS (weight)		
oz	ounces	28	grams	g
lb	pounds	0.45	kilograms	kg
	short tons (2000 lb)	0.9	tonnes	t
		VOLUME		
tsp	teaspoons	5	milliliters	ml
Tbsp	tablespoons	15	milliliters	ml
fl oz	fluid ounces	30	milliliters	ml
c	cups	0.24	liters	l
pt	pints	0.47	liters	l
qt	quarts	0.95	liters	l
gal	gallons	3.8	liters	l
ft^3	cubic feet	0.03	cubic meters	m^3
yd^3	cubic yards	0.76	cubic meters	m^3
		TEMPERATURE (exact)		
°F	Fahrenheit temperature	5/9 (after subtracting 32)	Celsius temperature	°C

*1 in = 2.54 (exactly). For other exact conversions and more detailed tables, see NBS Misc. Publ. 286, Units of Weights and Measures, Price $2.25, SD Catalog No. C13.10:286.

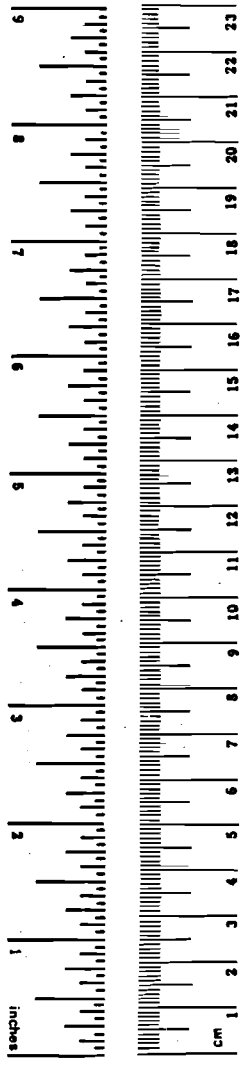

Approximate Conversions from Metric Measures

Symbol	When You Know	Multiply by	To Find	Symbol
		LENGTH		
mm	millimeters	0.04	inches	in
cm	centimeters	0.4	inches	in
m	meters	3.3	feet	ft
m	meters	1.1	yards	yd
km	kilometers	0.6	miles	mi
		AREA		
cm^2	square centimeters	0.16	square inches	in^2
m^2	square meters	1.2	square yards	yd^2
km^2	square kilometers	0.4	square miles	mi^2
ha	hectares (10,000 m^2)	2.5	acres	
		MASS (weight)		
g	grams	0.035	ounces	oz
kg	kilograms	2.2	pounds	lb
t	tonnes (1000 kg)	1.1	short tons	
		VOLUME		
ml	milliliters	0.03	fluid ounces	fl oz
l	liters	2.1	pints	pt
l	liters	1.06	quarts	qt
l	liters	0.26	gallons	gal
m^3	cubic meters	35	cubic feet	ft^3
m^3	cubic meters	1.3	cubic yards	yd^3
		TEMPERATURE (exact)		
°C	Celsius temperature	9/5 (then add 32)	Fahrenheit temperature	°F

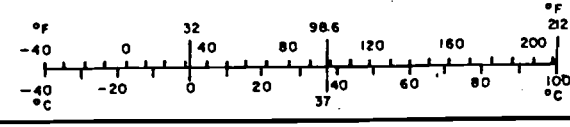

TABLE OF CONTENTS

		Page
I.	Introduction and Summary	1
II.	Principles of Electromagnetic Acoustic Transducer Operation	2
III.	Experimental Apparatus	7
	A. Rail Samples	7
	B. Electronics	8
	C. Electromagnet	8
	D. Motion Simulation Devices	13
	E. EMAT Construction	18
IV.	Results	24
	A. Low Frequency	24
	B. Medium Frequency	44
	C. High Frequency	53
V.	Conclusions	64
VI.	Acknowledgements	67
VII.	References	68
VIII.	Appendix A	69

LIST OF ILLUSTRATIONS

Fig. 1	Principles of Noncontact Transduction	3
Fig. 2	Generation of Surface Waves and Angle Bulk Waves	4
Fig. 3	Coil Configuration for 0° EMAT	5
Fig. 4	Electromagnet	9
Fig. 5	a) Polepiece #1, b) Polepiece #2, c) Polepiece #3	10
Fig. 6	Magnetic Flux Paths	14
Fig. 7	Field vs. Electromagnet Current Characteristics	15
Fig. 8	Field vs. Received Signal Amplitude	16
Fig. 9	Magnet Lift-off vs. Received Signal Amplitude	17
Fig. 10	Structure for Moving Small Rail	19
Fig. 11	Structure for Moving Long Rail	20
Fig. 12	Meander Coil	21
Fig. 13	Mid Frequency EMAT	22
Fig. 14	Arrangement of EMATs for Low Frequency Operation	25
Fig. 15	Block Diagram of the Low Frequency EMAT System	26
Fig. 16	a) RF Burst of Current, b) S/N for the Low Frequency EMAT	27
Fig. 17	Acoustic Signal Paths for Low Frequency Operation	28
Fig. 18	Display of End Reflection Signals for Low Frequency Operation	29
Fig. 19	Simulated Flaws	30
Fig. 20	Reflections from the Simulated Defects	31
Fig. 21	Detection Sensitivity for Normal and Tangential Fields	32
Fig. 22	Noise Level in the Low Frequency EMAT Receiver	34
Fig. 23	Echo Signals Observed in Rail No. 6 (Horizontal Splithead)	35
Fig. 24	Echoes from Transverse Fissures	36
Fig. 25	Reflection from Transverse Fissure in Rail No. 304	37
Fig. 26	Transverse Defects Observed in Rail No. 306	38
Fig. 27	Echo Observed from an Inclusion, # 302	39
Fig. 28	Echoes from Engine Burn Fracture # 309	41
Fig. 29	Reflections from Surface Shelling # 307	42
Fig. 30	Low Frequency EMAT Lift-off Characteristics	43
Fig. 31	Detection of Web Defects Using Medium Frequency EMAT	45
Fig. 32	Block Diagram of the Mid Frequency EMAT System	46
Fig. 33	Signal Strength, Different Frequency and θ Observed	47
Fig. 34	Comparison between Theory and Experiment for θ	48
Fig. 35	Angular Dependence of the Acoustic Energy	49
Fig. 36	Current Waveform and Base Reflection, Mid Frequency EMAT	51
Fig. 37	Reflection Observed from a Bolt Hole Crack	52
Fig. 38	Pulse-Echo Signal of Mid Frequency EMAT from Bolt Hole Crack	54
Fig. 39	Mid Frequency EMAT Lift-off Characteristics	55
Fig. 40	Block Diagram of the High Frequency EMAT System	56
Fig. 41	Transmitter Current, Receiver Noise for High Frequency System	57
Fig. 42	Identification of Bolt Hole Crack Using High Frequency EMAT	58
Fig. 43	Disappearance of Base Reflection by Head and Web Separation	59
Fig. 44	Disappearance of Base Reflection by Horizontal Split Head	60
Fig. 45	Disappearance of Base Reflection by Vertical Split Head	62
Fig. 46	High Frequency EMAT Lift-off Characteristics	63

LIST OF TABLES

Table 1. Short Rail Samples 7

Table 2. Long Rail Samples 7

Table 3. Comparison of Pole Pieces 9

Table 4. Result of the Overall Program 64

Table 5. Sensitivity Table 65

I. INTRODUCTION AND SUMMARY

This is the final report of the first phase of an investigation of the application of electromagnetic acoustic transducers (EMAT) to detection of flaws in railroad rails. The Federal Railroad Administration's Track Safety Standards define rail defects and conditions which inspections must detect (see Appendix A). The work described in this report used samples of flawed rails and laboratory EMAT equipment to verify that the EMAT technology is capable of detecting critical rail defects with sensitivities comparable to those of existing piezoelectric systems, but without requiring surface contact or a fluid coupling agent between the sensor and rail which the existing systems require. Sperry Rail Service assisted Rockwell International in defining operating requirements for operational inspection systems, and supplied flawed rails with piezoelectric analysis data for comparison with EMAT results.

The EMAT devices used in this work consisted of a flat electromagnetic coil suspended in a strong static magnetic field close to the rail to be inspected. Radio frequency pulses in the EMAT coil generate eddy currents in the rail surface. The interaction of the eddy currents and the static magnetic field generates ultrasonic energy which is beamed within the rail, and produces echo signals from cracks and other irregularities in the rail. The returning echoes interact with the magnetic field at the rail surface, creating an echo pulse in the EMAT coil which can be used to determine the presence and magnitude of defects encountered by the beam.

The work described in this report was an initial feasibility study of the potential of EMAT systems for rail inspection. Rail sections containing known flaws in both their head and web sections were subjected to inspections with laboratory EMAT equipment. EMAT coil configurations, operating frequencies, power levels, and static magnetic field configurations and strengths were varied to determine EMAT operating characteristics on differing rail geometries and materials. All critical rail defects supplied for test were detected with the laboratory EMAT, with sensitivities comparable to those obtained with conventional piezoelectric ultrasonic inspection methods. Acceptable signal levels were obtained at separations ("lift-offs") of up to 1/16 inch between the EMAT coil and the rail head. Signal degradation of some of the flaw signals became excessive at greater lift-offs. Separations of up to $\frac{1}{2}$ inch between the static field electromagnetic pole pieces and the rail head were found to be acceptable. These results demonstrate that the EMAT technology has potential for development into a high-speed, high-reliability rail flaw detection system.

Subsequent phases of this research effort will concentrate on optimization of EMAT operating parameters, confirmation of the detectability of all critical rail flaws, and engineering of EMAT systems which can operate successfully in the railroad environment.

II. PRINCIPLES OF ELECTROMAGNETIC ACOUSTIC TRANSDUCER OPERATION

Figure 1 illustrates the basic principles of the electromagnetic acoustic transducer (EMAT) which can excite and detect ultrasonic waves in a metal without a couplant medium. When a wire carrying a dynamic current is placed adjacent to a metal part, eddy currents are induced within the material. If, in addition, a static magnetic field is present, these induced currents will experience a force (as in an electric motor) which launches ultrasonic waves. Conversely, if the surface of the material is moving as a result of an ultrasonic wave impinging upon it from some remote location, there will be eddy currents induced in the metal as it moves in the static magnetic field (as in an electric generator). These currents will be inductively detected by the wire and appropriate electronic receivers. Hence, the same transducer structure (a coil of wire and a magnet) can be used either as a transmitter or a receiver, to both excite and detect ultrasonic waves in metals without making physical contact with the metal. This noncontact feature permits applications of the transducer in situations where the part to be inspected with ultrasonic waves is moving rapidly past the transducer. An excellent example of this feature would be in the rapid inspection of railroad track. By bending the wire shown in Fig. 1 into a coil of various shapes, various different kinds of sound waves can be generated.

In order to launch and detect surface and angle beam shear waves, the transducer coil is wound in a meander, or serpentine fashion as shown at the top of Fig. 2. If such a coil, along with the magnet necessary to produce the static field (not shown), is placed on the material surface, either of these two wave types can be selected by appropriate variation of the frequency. When the frequency f is chosen according to the relation:

$$f = \frac{V_R}{2D} \tag{1}$$

where D is one half the meander coil period and V_R is the Rayleigh (surface) wave velocity, surface waves will be most efficiently generated, since their wavelength is just equal to the coil period. At higher frequencies, angle shear waves can be generated, since the shorter wavelength can still match the coil period when the wave is traveling at an angle into the material as shown in the bottom of Fig. 2. This angle measured with respect to the surface normal is given by:

$$\theta = \sin^{-1}(V_S/2fD) \tag{2}$$

where V_S is the shear wave velocity.

In order to excite plane waves normal to the metal surface, an EMAT coil arrangement similar to that shown in Fig. 3 can be used. The eddy currents

PRINCIPLES OF NONCONTACT TRANSDUCTION

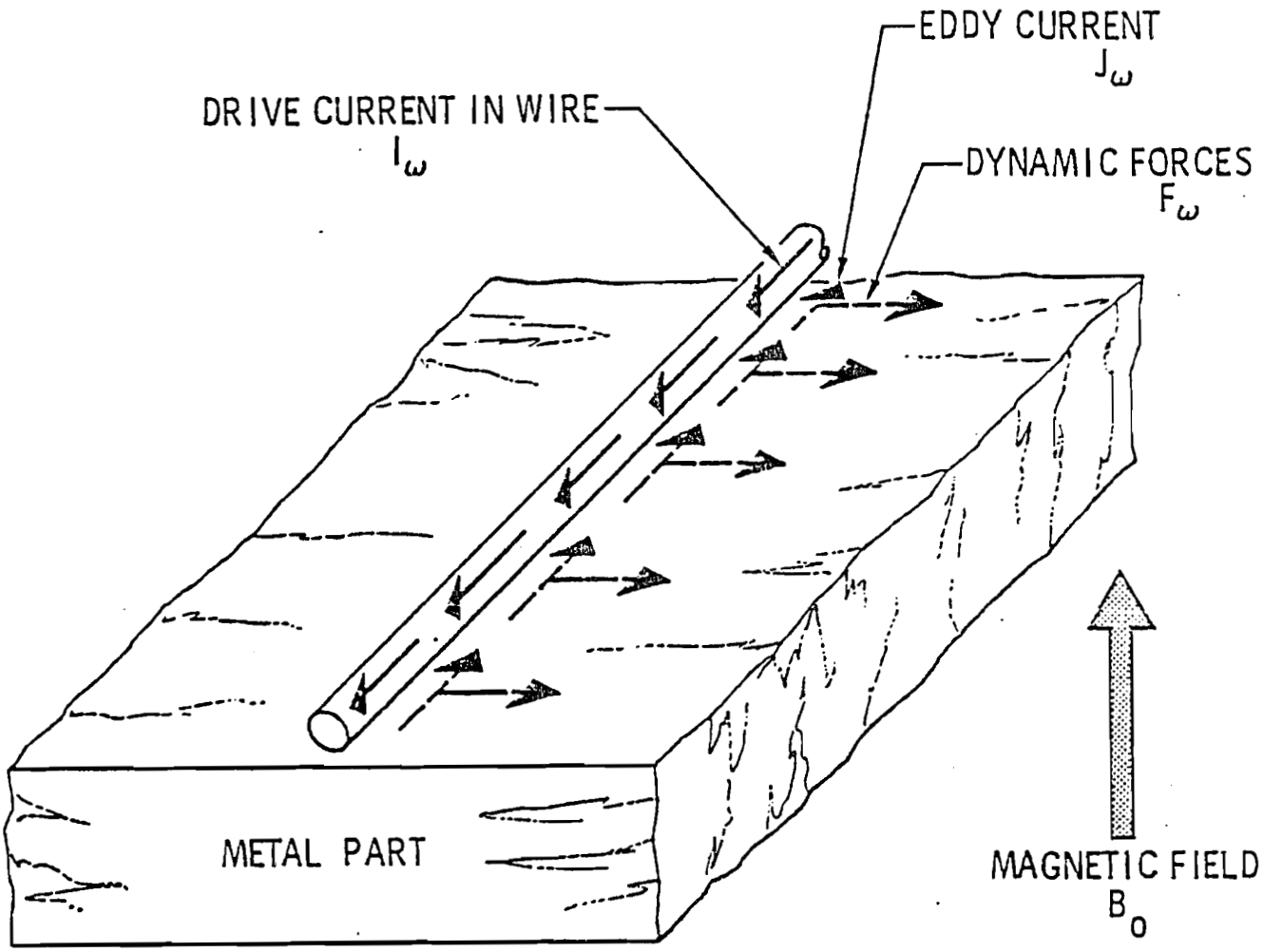

LORENTZ FORCE
(AS IN ELECTRIC MOTOR)

$$\vec{F}_\omega = \vec{J}_\omega \times \vec{B}_0$$

Fig. 1 Distribution of currents and forces on the lattice of a metal part contributing to generation of ultrasonic signals under normal field bias.

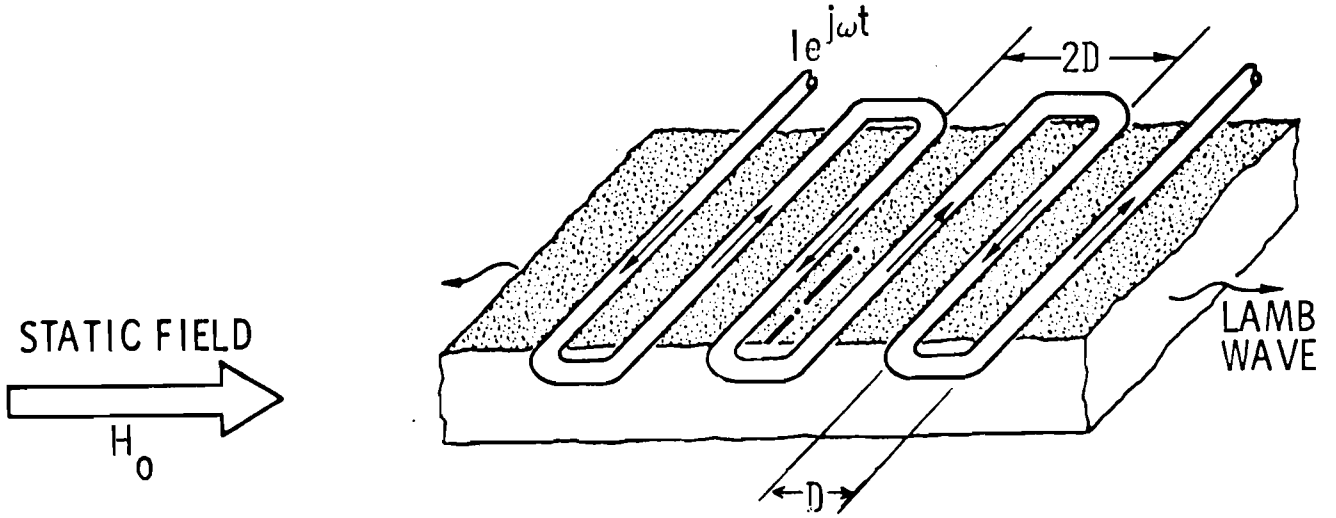

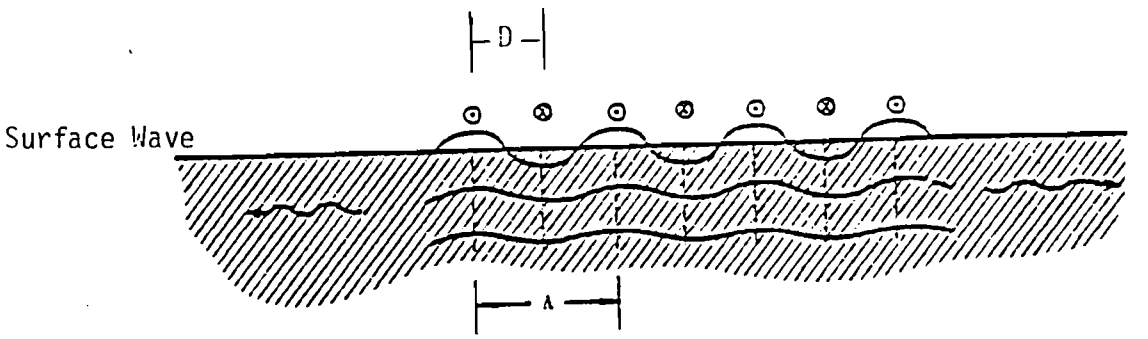

ANGLE SHEAR WAVES: $\phi \approx \sin \frac{-1\ Vs}{2\ f\ D}$

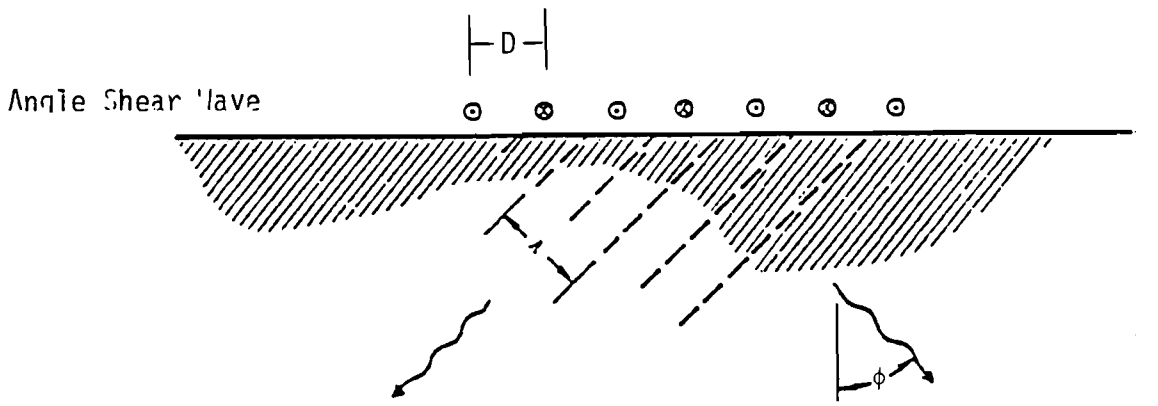

Fig. 2 Principle of generation of surface waves and angle bulk waves by meander coil electromagnetic transducers.

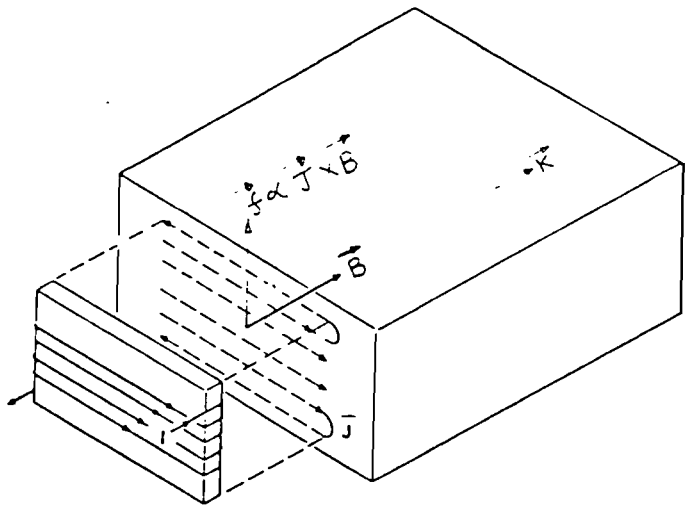

Fig. 3 EMAT coil configuration for normal acoustic wave generation in the bulk of a solid.

are schematically indicated by dashed arrows on the face of the sample. In accordance with the motor rule, shear waves are generated when the static magnetic field is normal to the sample face and compressional waves are generated when the field is in the plane of the face but normal to the eddy currents. The same configuration can act as a receiver.

The ratio of electrical voltage V generated at a receiver transducer to the drive current I in an identical transmitter transducer is given by:

$$\frac{V}{I} = \frac{2N^2Bo^2A}{\rho v} \tag{3}$$

where N is the number of wires per unit width of the transducer, I is the dynamic current in the transmitter coil, ρ is the density of the metal, v is the ultrasonic velocity in the metal, Bo is the applied magnetic field, and A is the transducer area. Note that any spreading or attenuation of the acoustic beam has been neglected.

The power conversion efficiency, E, defined as the ratio of radiated acoustic power to the electrical power available in the generator, is given by:

$$E = \frac{4N^2Bo^2RoA}{\rho v(R+Ro)^2} \tag{4}$$

where R is the resistance of the transducer and Ro is that of the generator.

Comparisons of measured performance to the theoretical typically differ by only 10 dB after corrections for the attenuation in the sample have been taken into account.

It is clear from Eqn. 4 that the highest efficiencies are to be obtained when the static magnetic field, Bo, is maximized and the resistance of the generator, Ro, is made comparable with the transducer resistance R. Increasing the number of turns, N, would also increase the efficiency, but the coil resistance R would also increase. If the resistance per turn, R/N, is minimized, the efficiency is improved; so it pays to use large copper wires in the transmitter EMAT.

III. EXPERIMENTAL APPARATUS

A. Rail Samples

Sperry Rail Service has cooperated with various railroads to procure samples of rails which contained various defects. They also used their facilities and trained personnel to locate the flaws in each rail and to identify its type and size. The rails ranged in length from 2 feet long to over 10 feet. The short (2 to 3 foot long) rails were difficult to inspect by EMATs which launch acoustic waves along the head since acoustic reflections from the ends of the rails tended to interfere with the flaw signals. Most of the samples, however, avoided the problem because they had lengths of 8 to 10 feet. The tables below describe the rails that were received and tested by the end of this initial program Phase (A). The brief description of the types of rail defects are given in the Appendix.

Table 1 Short Rail Samples

Sperry Rail Number	Defect Type	Defect Length
6	Horizontal split head	7"
6	Crushed head	7"
219-HW	Head/web separation	7"
219-F	Weld repair	4"
32	Bolt hole crack	2"

Table 2 Long Rail Specimens

Sperry Rail Number	DOT Defect Type	Sperry Rail Label	Remarks
#302	Head inclusion	D.W.P.	Curve worn rail
#303	Transverse fissure	T.D.T.	True trans. def., small
#304	Transverse fissure	T.D.D.	High in the head
#305	Transverse fissure	T.D.T.	Head free rail
#306	Transverse fissure	T.D.D.	Deep in head
#307	Surface shelling		Also has exposed T.D.D.
#308	Transverse fissure	T.D.D.	Possible compound & good gas weld

Table 2 Long Rail Specimens (Continued)

Sperry Rail Number	DOT Defect Type	Sperry Rail Label	Remarks
#309	Engine burn fracture	E.B.F.	Crack is visible
#310	Vertical split head	V.S.H.	Approx. 24" long
#311	Vertical split head	V.S.H.	Approx. 24" long (head freerail)

T.D.T. stands for True Transverse Defect
T.D.D. stands for Detailed Fracture Transverse Defect
D.W.P. stands for Defective Weld Plant

All rails were heavy rail (130 or 132 lbs. per yard).

B. Electronics

The electronic components necessary for operating the special EMATs prepared for this program consisted of high current, low output impedance transmitters for driving the transmitter EMATs and low noise preamplifiers with unusually low input impedance for attachment to the EMAT receivers. Both of these circuits were already available at the Albuquerque Development Laboratory from other programs. Additional components such as signal generators, oscilloscopes and cameras were commercial instruments also available in the laboratory. For the acoustic pulse signals, pulsed RF bursts consisting of 5 to 15 cycles were fed to the EMAT transmitters with a pulse repetition frequency of up to 100 hz. The EMAT coils attached to the transmitter and receiver were similar in configuration.

C. Electromagnet

The electromagnet for supplying the static magnetic field to the EMAT coils is shown in Figure 4. It has an iron core 2" x 6" in cross section (12 sq. in. area) and had two encircling coils consisting of 1700 turns of #12 copper wire each. At its normal operating condition it drew 6 ampers and dissipated 300 watts of electrical power. Its total weight was approximately 315 lbs. This electromagnet was already available at the Albuquerque Development Laboratory and proved to be quite adequate for the experiments performed in the program. However, future programs will probably require a somewhat different electromagnet designed to fit under a rail inspection car and possibly capable of delivering more magnetic flux through the EMAT to the rail.

It was learned that the pole pieces which attach to the electromagnet and "focus" the magnetic flux into the rail head played a very significant

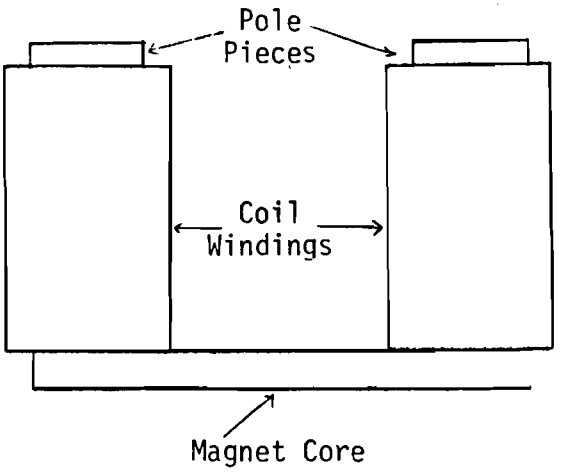

Fig. 4 Electromagnet used to generate the static magnetic field required by the EMATs.

role in the performance of the EMATs. In the earliest experiments, a simple flat slab pole piece, shown in Fig. 5(a), was used because many different EMAT shapes were experimented with. Later, the tapered and curved pole piece shown in Fig. 5(b) was used to achieve high fields normal to the rail head in the gap between the rail and the magnet. For the small, high frequency EMATs examined near the end of the program, the pole piece shown in Fig. 5(c) was used. Table 3 compares the performance characteristics of these three pole pieces.

Table 3 Comparison of the Performance Characteristics of Various Pole Piece Designs at a 1/4" Gap Between the Rail and the Pole Piece

No.	Field at 6 amps	Measured EMAT Signal	Figure
1	5 Kgauss	0 db	5(a)
2	7.5 Kgauss	+5 db	5(b)
3	12 Kgauss	+15 db	5(c)

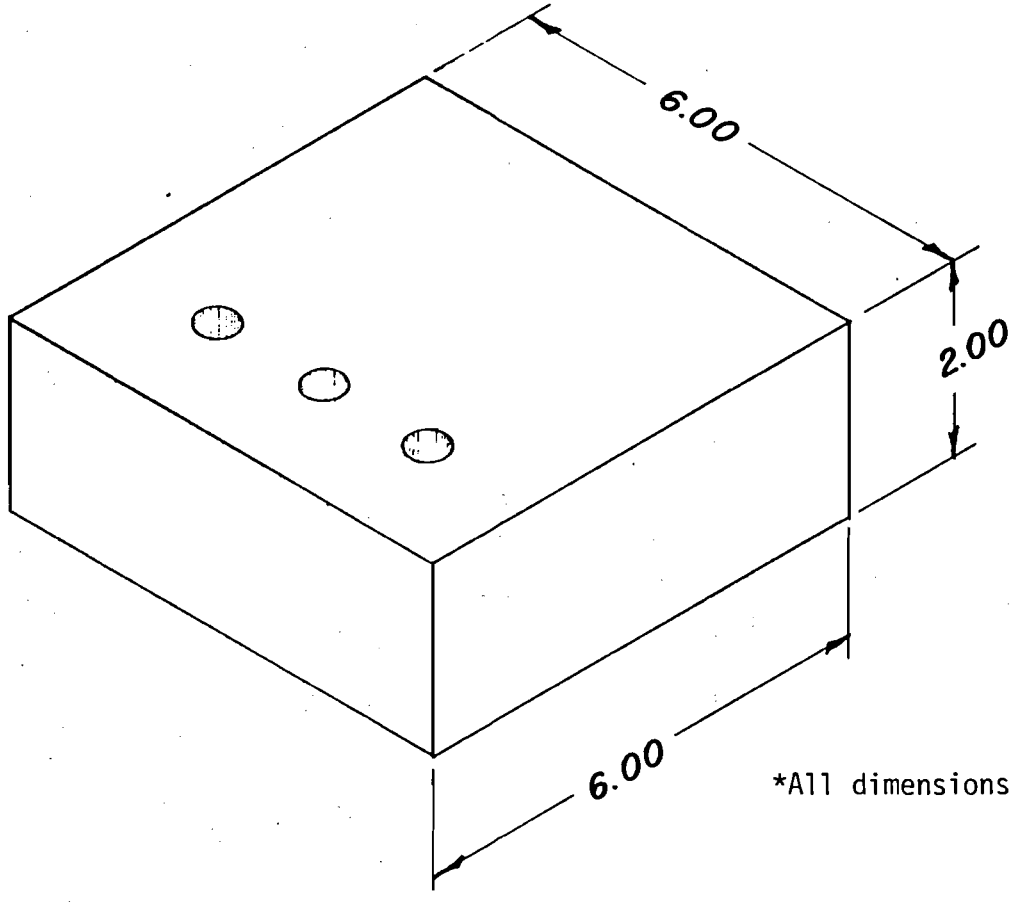

Fig. 5(a) Pole Piece #1 EMAT mounts on the top surface.

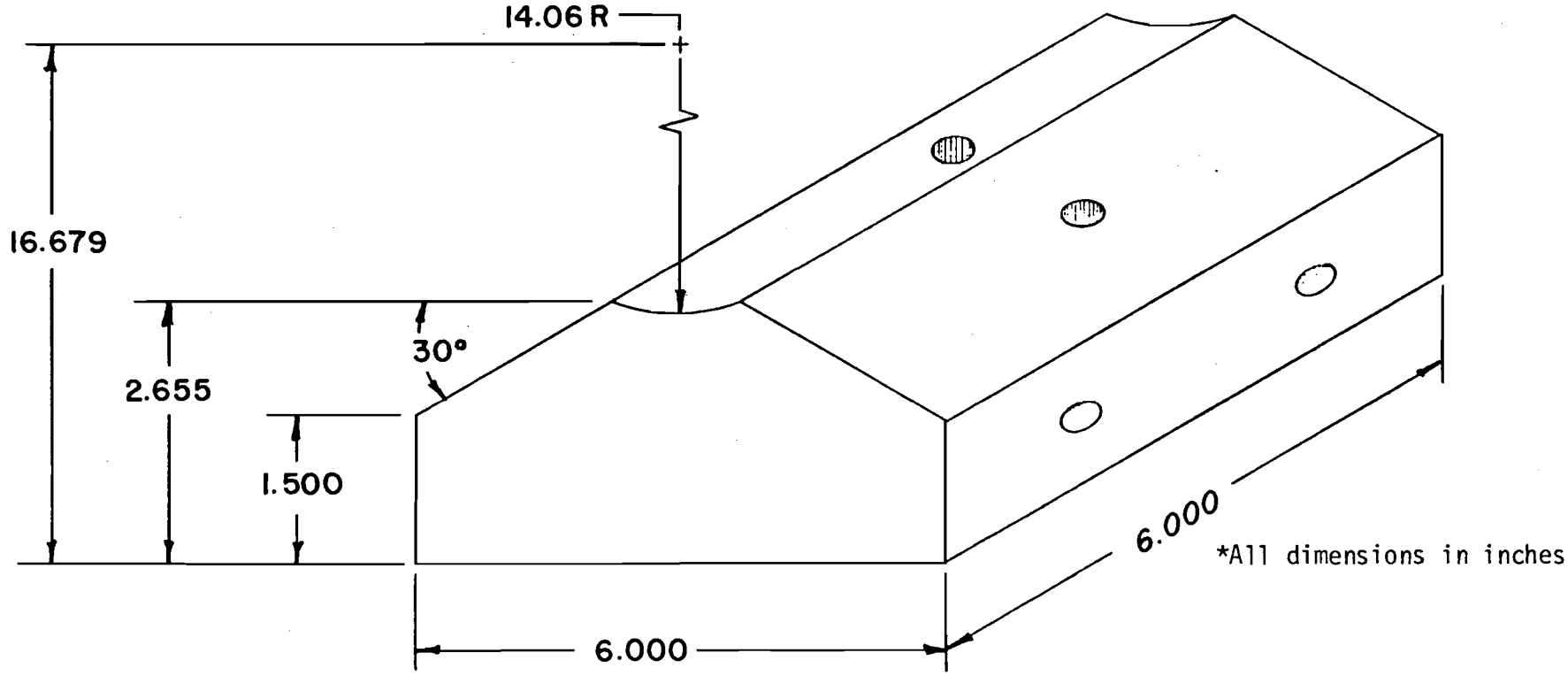

Fig. 5(b) Pole piece #2 EMAT mounts on the top surface.

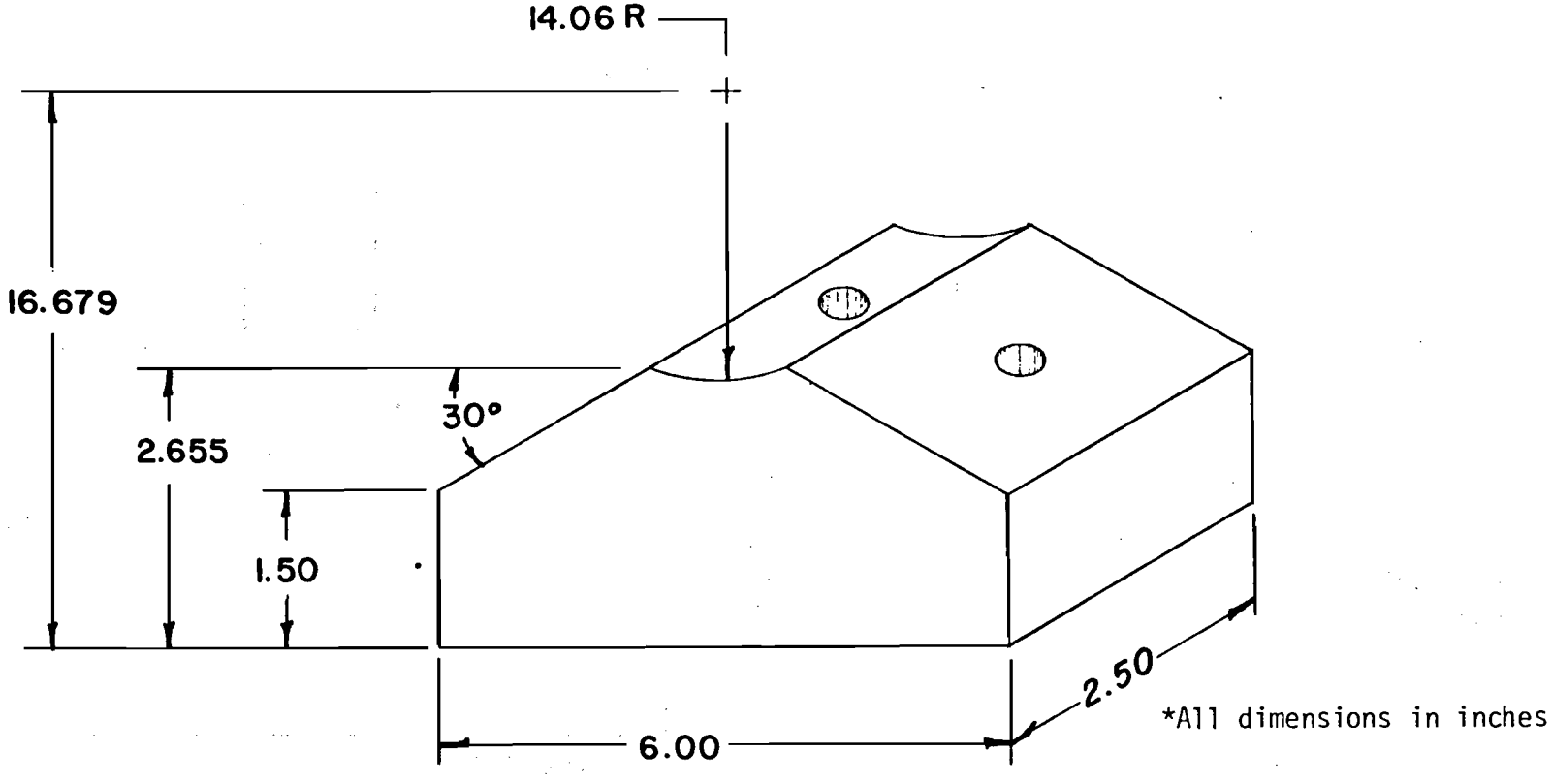

Fig. 5(c) Pole piece #3 EMAT mounts on the top surface.

Figure 6 shows schematically how the magnetic flux flows from the electromagnet pole pieces into the rail. EMATs were placed either in the gap between the pole piece and the rail where they operated in a normal magnetic field or in between the two pole pieces where the magnetic field was tangential or parallel to the rail head's longitudinal axis. Depending upon the magnetic characteristics of the different rail materials tested, slightly different magnetic fields were observed at the same current level in the electromagnet as is shown in Figure 7 for rails 6 and 219 (see Table 1). The measured tangential field is smaller because it was measured by a Hall probe held outside the rail head where there is an H field (Inside the rail, the magnetic induction B field is the permeability of iron multiplied by the H field).

Figure 8 shows the dependence of the total generation-reception efficiency of an EMAT transducer pair as a function of magnetic field for two different rail samples. Figure 8(a) shows the results obtained when the EMATs were placed in the gap beneath the pole piece where the field is presumably normal to the rail head and Figure 8(b) shows the signals from EMATs located between the pole pieces--under nominally tangential magnetic field conditions. A gap field of 5 to 6 KG corresponds to an equivalent tangential field of 50 to 60 G. The important feature to perseve is that for normal fields the signal levels obtained on these two different rail specimens are approximately the same (within 25%). However, for the tangential field configurations, gross signal level differences are observed for rail #219 compared to #6. Vastly different EMAT efficiencies have been observed in inspection of other kinds of ferromagnetic samples (inspected on other EMAT programs) and is understood to arise due to magnetostrictive contributions to the transduction process which are critically dependent upon the track manufacturing process, its stress history, and its chemical nature (percent carbon content). Since there is so much variability in EMAT coupling in the tangential inspection case, it is advisable to always operate EMATS in the normal field configuration. Thus EMAT inspection signals derived from normal magnetic field operation should be effected only minimally by differing (real world) rail conditions.

In an actual inspection system, the massive electromagnet and its pole pieces will have to be held as far from the rail head as possible to prevent damage from physical contact with the track structures. The light EMAT coils should be as close as possible to the rail and their mechanical design will have to be such that they can servive some contact with the rail. Figure 9 shows how the efficiency of a single EMAT when the gap between the rail and the pole piece is varied with the location changes of the EMAT held fixed. It is obvious that satisfactory performance of the EMAT can be achieved even when the pole piece is a half inch or more removed from the rail.

D. Motion Simulation Devices

In order to simulate the motion of the rail past the EMATs and electro-

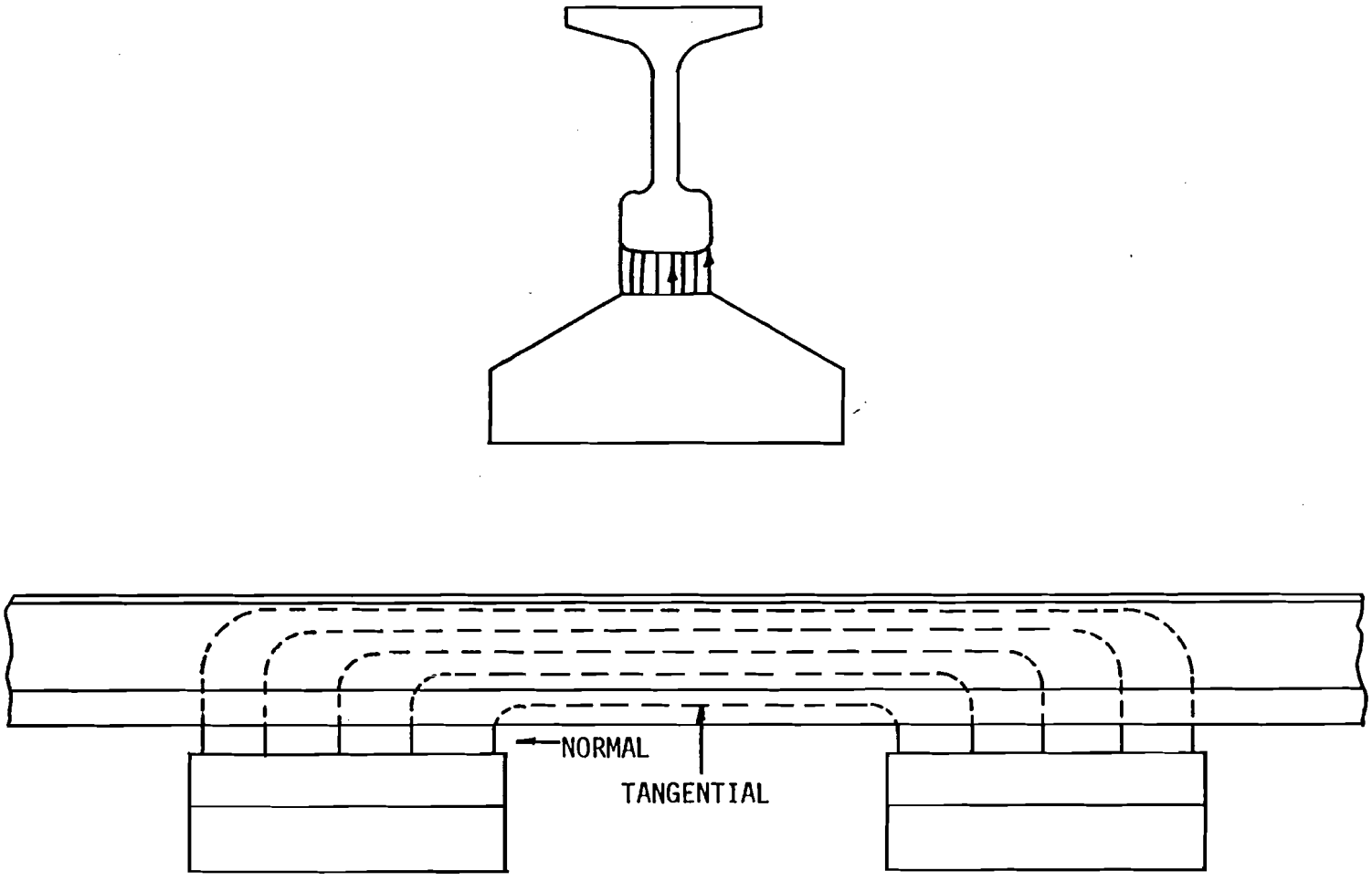

Fig. 6 Diagram showing magnetic flux paths in the rail from the electromagnet pole pieces.

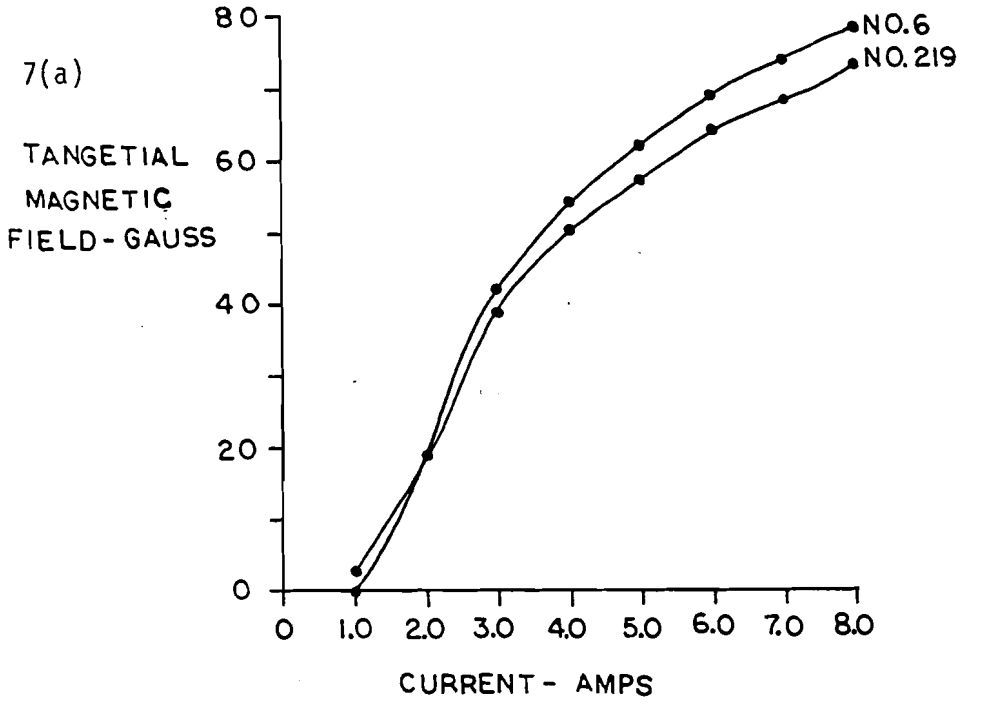

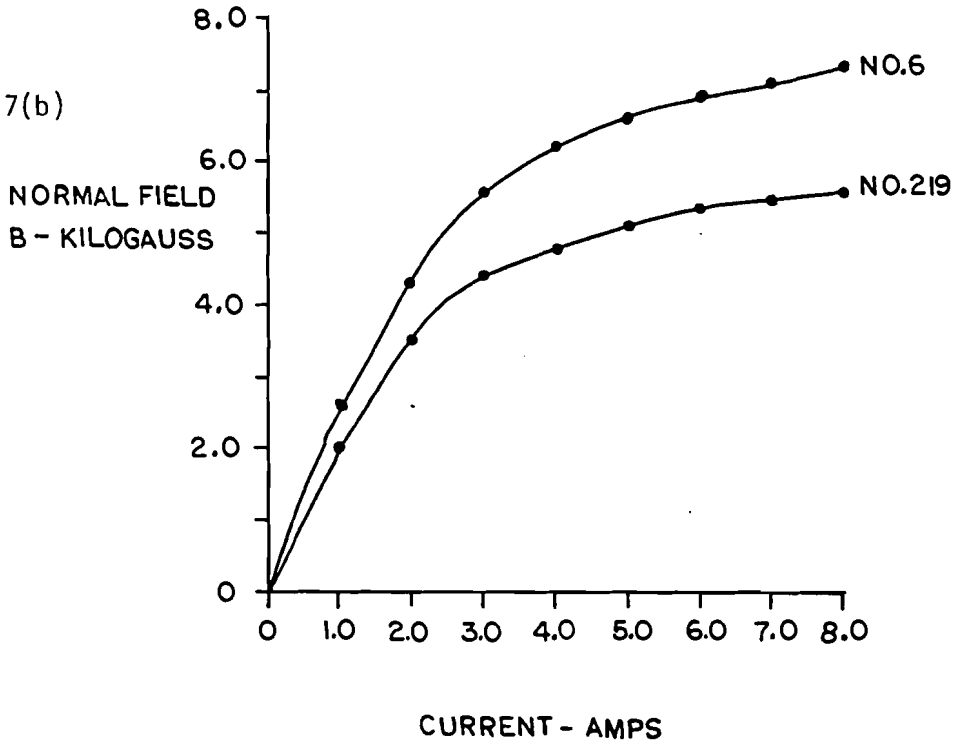

Fig. 7 Field versus electromagnet current characteristics observed with pole piece #2 on rails #6 and #219 with a 0.31" gap between the pole piece and the rail head. (a) Tangential field, (b) Normal field.

8(a)

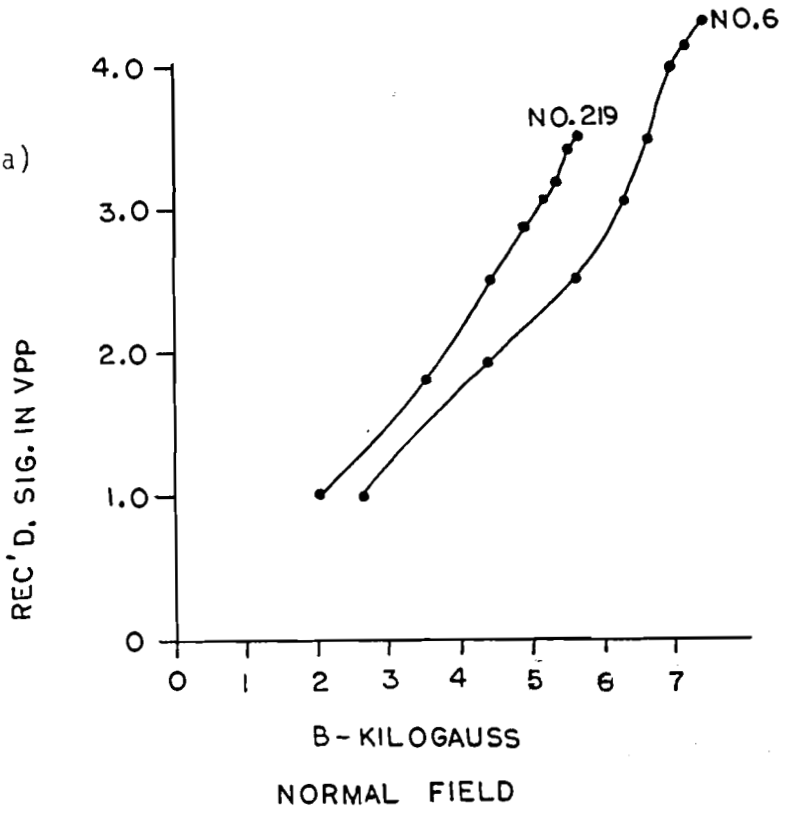

8(b)

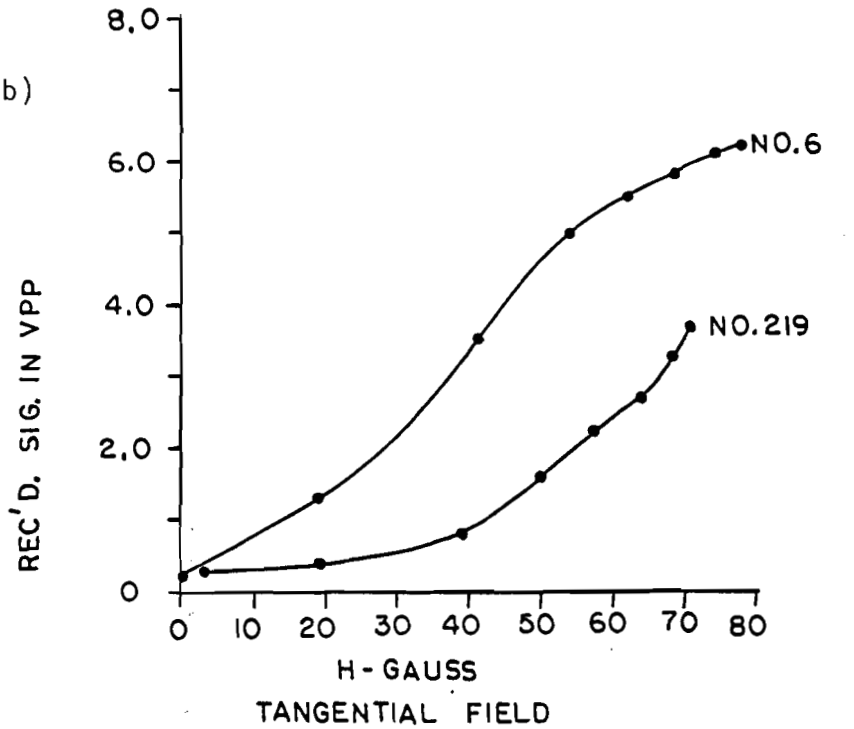

Fig. 8 Using pole piece #2, EMAT signals observed as a function of magnetic field at the EMAT for two orientations of the field and for two rails. (a) Normal field, (b) Tangential field.

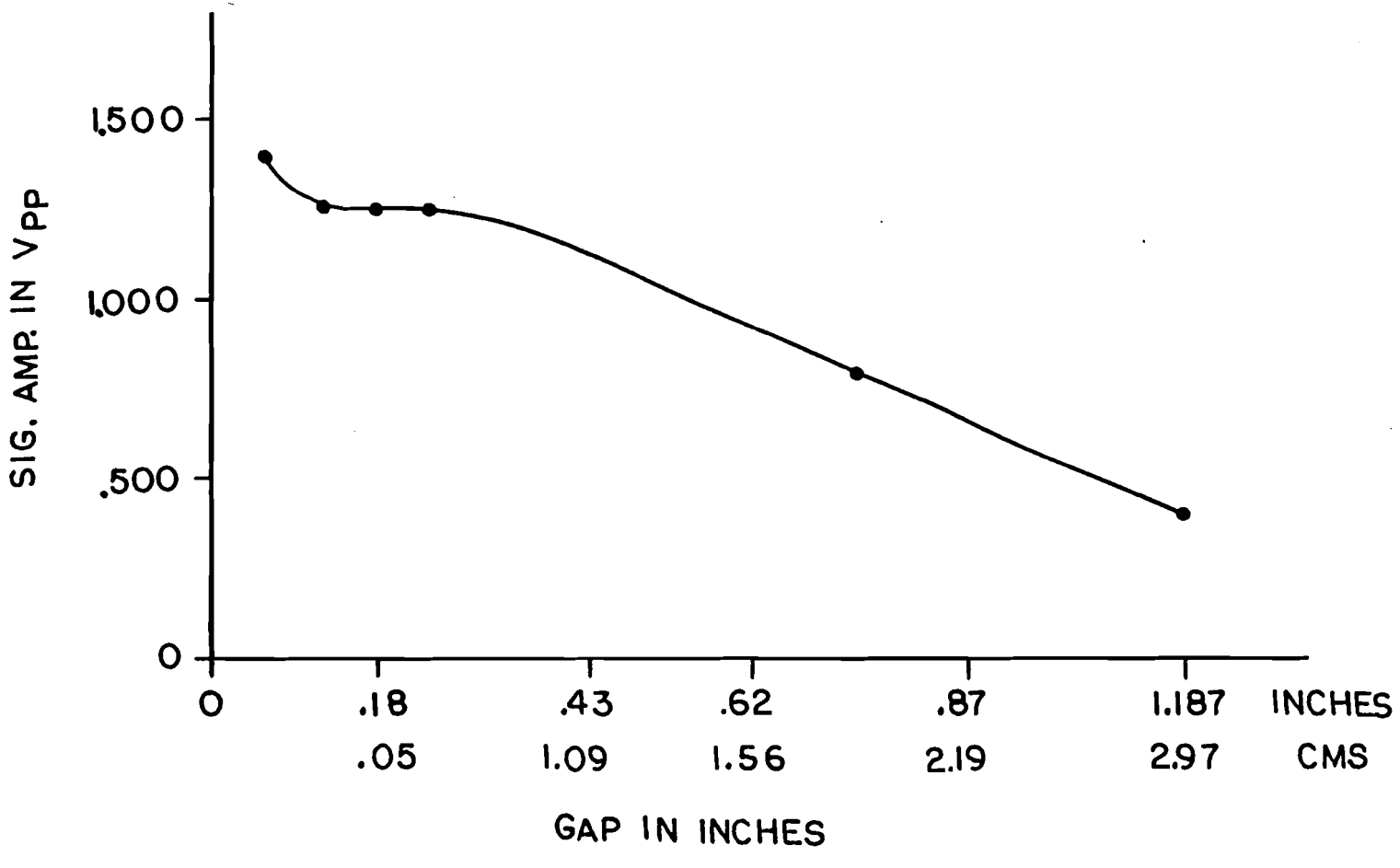

Fig. 9 Variation of the received signal amplitude as a function of the distance between pole pieces and rail while keeping the transducer close to the rail head using pole piece #1.

magnet as well as to observe how the defect signals change as the defective region approaches or recedes from the EMAT, special frames were constructed to support the rail over the electromagnet and to permit motion of the rail past the EMAT. For the short rails described in Table 1, a simple attachment was made to hold the pole pieces of the electromagnet. This simple device is shown in Figure 10 and consisted of a pair of wheels held over each pole piece to support the base of the rail. For the long rails, a bridge-like structure was used with rollers to support the rail a long way from the electromagnet and to maintain the alignment of the rail as it moved past the pole pieces. This longer structure is shown in Figure 11. In both cases, the rollers could be adjusted to accommodate rails of different dimensions. Motion of the rail was achieved by pushing or pulling the rail along by hand and no magnetic drag effects were observed because the speeds were always slow.

E. EMAT Construction

One of the attractive features of EMATs is that they are easily constructed from simple coils of wire. Therefore, many different sizes and shapes were constructed as demanded by the particular need. For the low and intermediate frequencies, the meander shape described in Figure 2 was used while the flat coil shape shown in Figure 3 was used for the high frequency studies. The coil form was a simple pc board or a piece of stiff cardboard on which the coil wires were laid down and held in place with adhesive. By using this technique, the EMATs could be adjusted to conform to the shape of the rail head. Figure 12 shows the outline of the meander coils used at low frequencies. The spacing D between adjacent conductors was chosen to define the wave length of the desired acoustic wave. In use, the frequency of the drive current was adjusted to excite the desired wave by meeting the conditions given in Equations 1 and 2 in Section II. Since the lift-off sensitivity of an EMAT depends upon the dimension D (more lift-off is tolerate for large values of D), a series of six EMATs were constructed with D = 0.25 cm, 0.5 cm, 0.7 cm, 1.5 cm, 2 cm, and 3 cm in order to determine exactly how much lift-off could be tolerated.

For intermediate frequencies an EMAT with D = 0.5 cm was constructed, as shown in Figure 13. This particular EMAT incorporated an additional feature of EMATs which allows a transmitter and receiver to be mounted on the same form. If the receiver wires are placed exactly midway between the transmitter wires (as shown in Figure 13) there will be no coupling between the two coils and the receiver does not have to be designed to accommodate the full power of the transmitter (in order to achieve transmit/receive operation in a single transducer). By tuning the EMAT in Figure 13 to frequencies which satisfy Equation 2 in Section II, the acoustic waves it excites and detects can be at an angle relative to the normal to the rail head. This angle beam feature is highly useful for inspecting the ends of the rail for cracks around bolt holes.

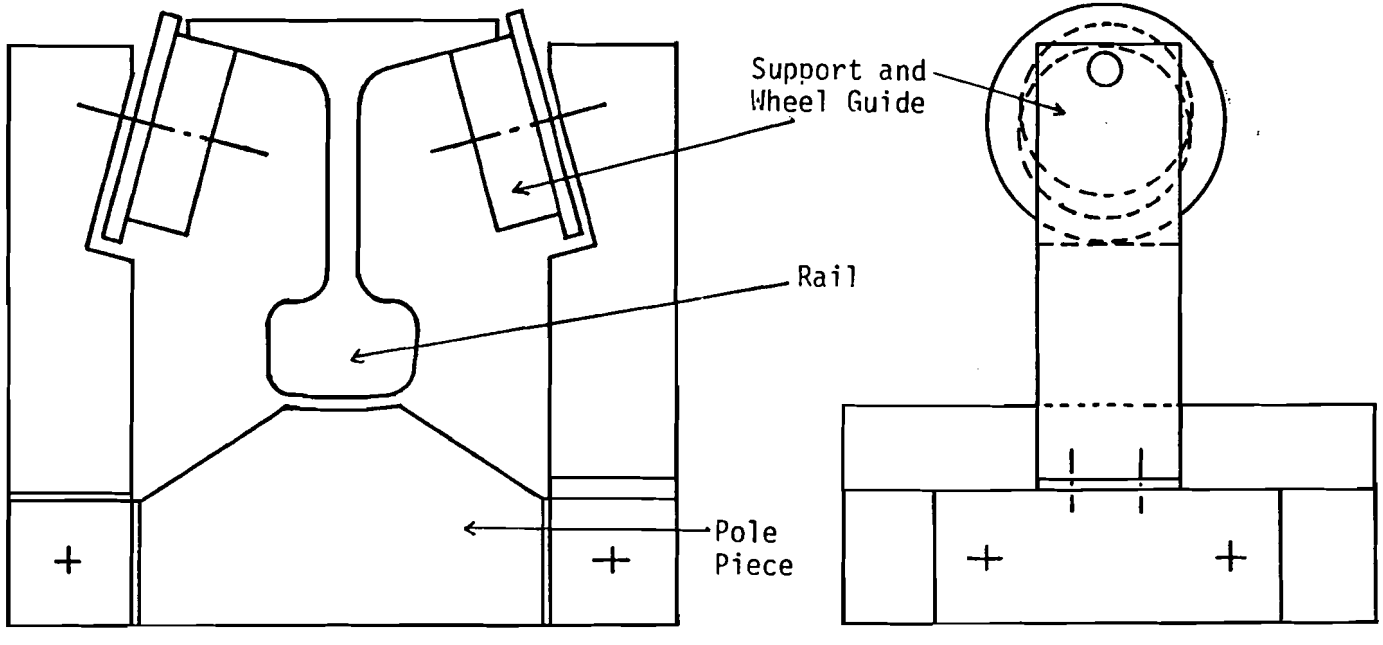

Fig. 10 Structure used for moving short rail specimens past the electromagnet.

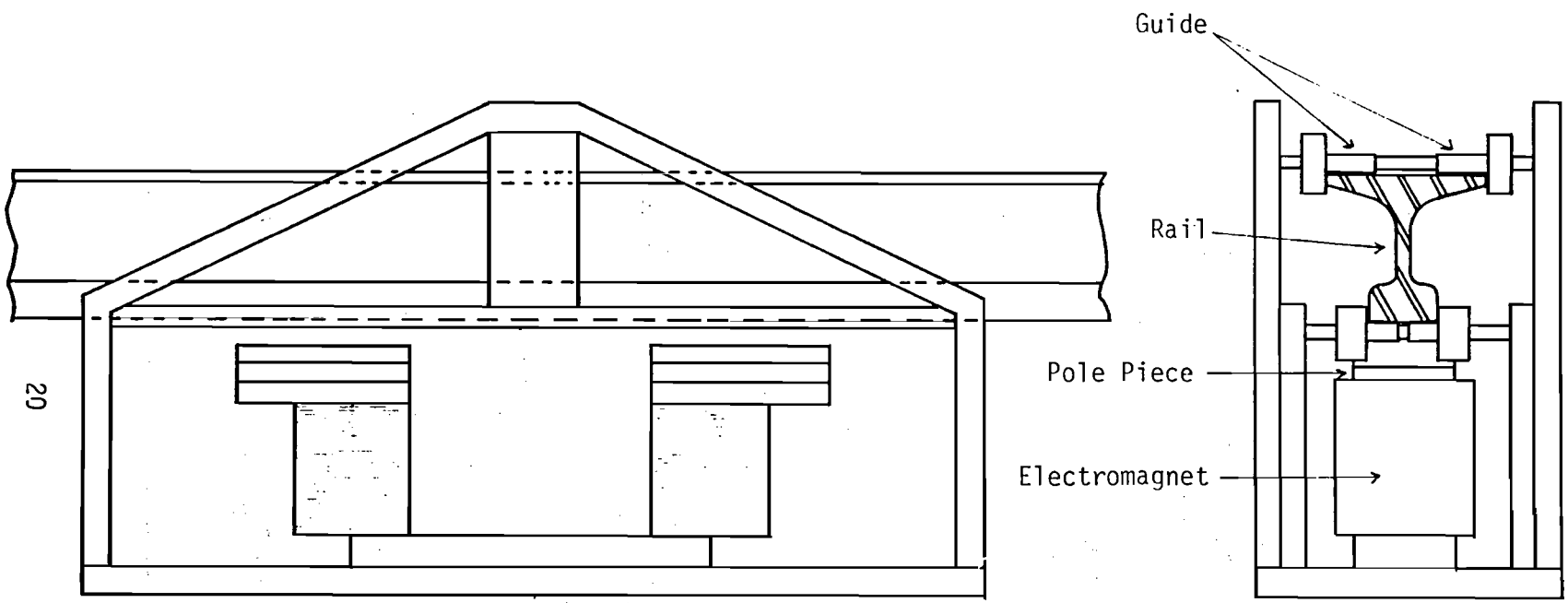

Fig. 11 Long rail moving system.

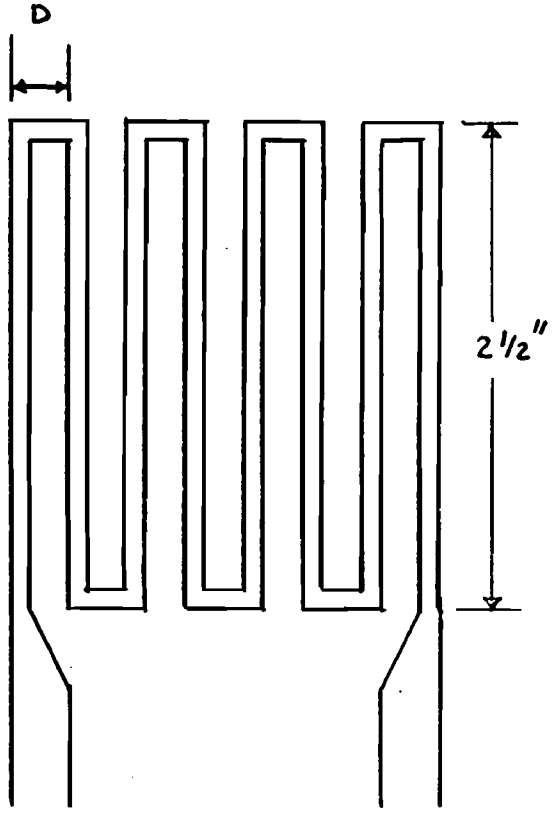

Fig. 12 Meander coil used at low frequency. The Spacing D was changed to study the properties of acoustic waves at different wave lengths and frequencies.

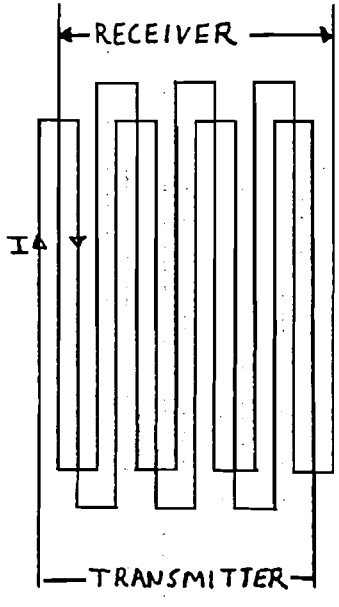

Mid Frequency EMAT
D = 0.5 cm
f = 560 KHz

Fig. 13 Arrangement of wires in a transmitter/receiver EMAT used at intermediate frequencies to launch and receive angle beam shear waves. Wire spacing D = 0.5 cm.

At high frequencies, a transducer was designed to excite acoustic waves vertically into the rail. By monitoring the disappearance of the reflection from the base of the rail it was found that normal (vertical) acoustic waves are quite sensitive to defects occurring in the web and base regions. This transducer had the form shown in Figure 3 of Section II. In order to concentrate the eddy currents in the rail head, an insulated copper sheet was placed so that the rail would be shielded from the oppositely flowing currents on the top side of the coil. When operated at 2 MHz, this coil produced shear waves propagating through the rail directly from head to the base with a wavelength of 0.041 inches (0.16 cm).

IV. RESULTS

A. Low Frequency

The motivation for investigating low frequency EMATs was two-fold. First, since lift-off insensitivity is proportional to wave length, the longer wave lengths associated with low frequencies should provide EMATs with good lift-off characteristics. Second, simple meander coil EMATs can easily launch acoustic waves along the head of the rail (at 90 degrees to the rail normal direction) and hence would have considerable advantages over the 70 degree piezoelectric transducers now being used to detect transverse defects in the rail head. Also, if the acoustic wavelength were comparable to the thickness of the rail head, they should be sensitive to defects buried inside the head. To test these features, the arrangement of EMATs shown in Fig. 14 was constructed. Either normal fields or tangential fields could be examined and transmitter EMATs could be separated from receiver EMATs. Figure 15 shows a block diagram of the electronic components used for the low frequency studies, and Fig. 16 displays the quality of the electronic signals observed on the oscilloscope for the case of 220 KHz operation (wave length = 1.4 cm). Figure 16 (a) shows the tone burst of current fed to the transmitter, and Fig. 16 (b) shows the output of a receiver EMAT placed some distance from the transmitter so that the acoustic signal would be time-resolved from the radiated electromagnetic transmitter signal (sometimes termed the "main bang").

Since these low frequency studies were performed early in the program, a wide variety of EMAT arrangements and frequencies were examined in order to gain experience with EMAT systems. Figure 17 shows a schematic of the relative transducer placement and illustrates the multiplicity of acoustic signals that are observed due to various reflections. Figure 18 presents the oscilloscope display corresponding to the EMAT arrangement in Fig. 17 at two frequencies and wavelengths using pole piece No. 1. The reflective echo pulses that are listed refer to those shown in Fig. 17. The low frequency operation leads to broader echoes and a reduced signal-to-noise ratio. In order to observe how defects in the rail affect the observed signals, three slots were cut into the head of a nominally unflawed rail sample, as shown in Fig. 19. Figure 20 shows the received acoustic reflection of these three defects as they appear on the oscilloscope trace for two relative positions of the EMATs. At long distances, approximately 30 inches, all three reflections are spaced in time so that they are resolved. As the EMAT approaches the slots, within 18 inches, the number 2 signal merges with the main bang signal so that the number 2 signal is not resolved. In all measurement instances, the EMATs were designed to be wider than the width of the head of the rail. Thus centering the acoustic beam to cover the entire head was not found to be critical in any rail samples tested.

The flaw detection sensitivity of EMATs as a function of magnetic field orientation was investigated as shown in Fig. 21. Here, flaw No. 2 (Fig. 19)

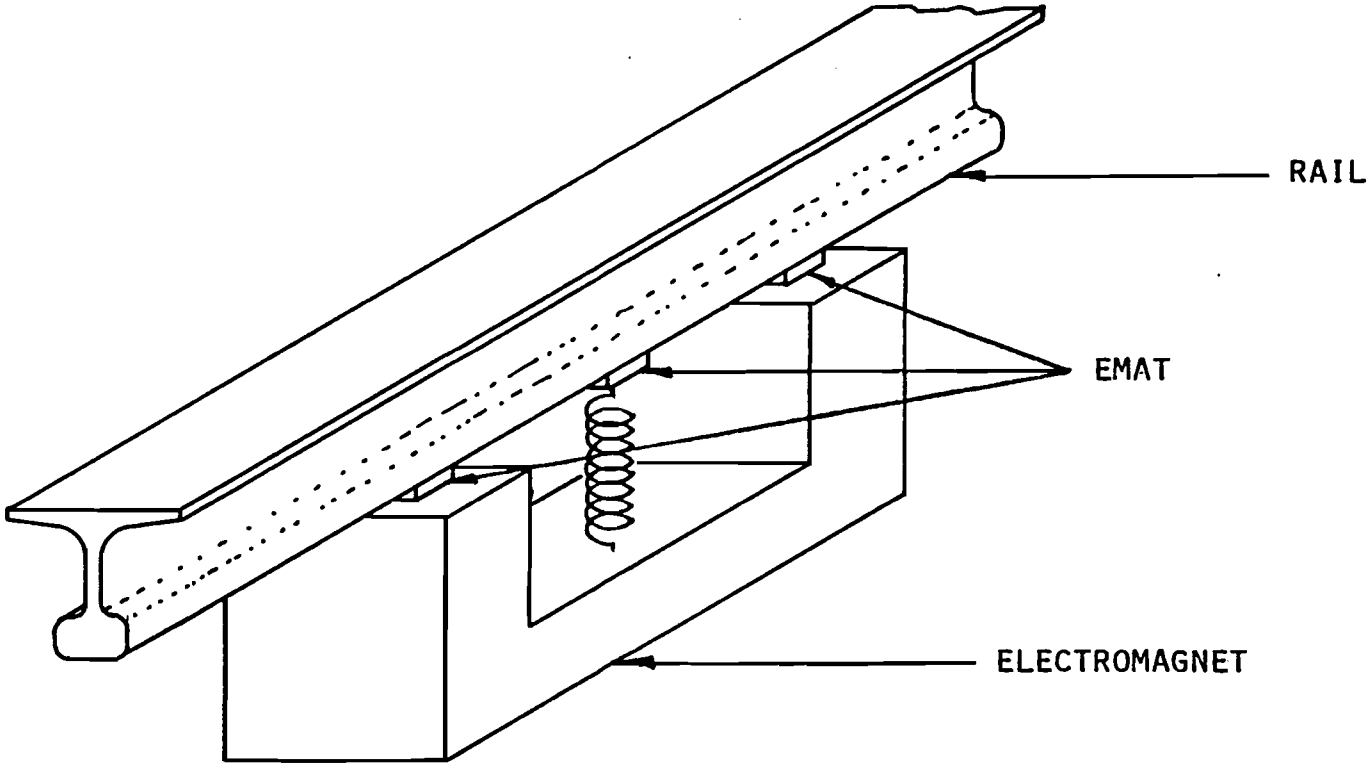

Fig. 14 Diagram showing the possible arrangement of EMATs for low frequency studies. Note that both normal and tangential field configurations are available for examination.

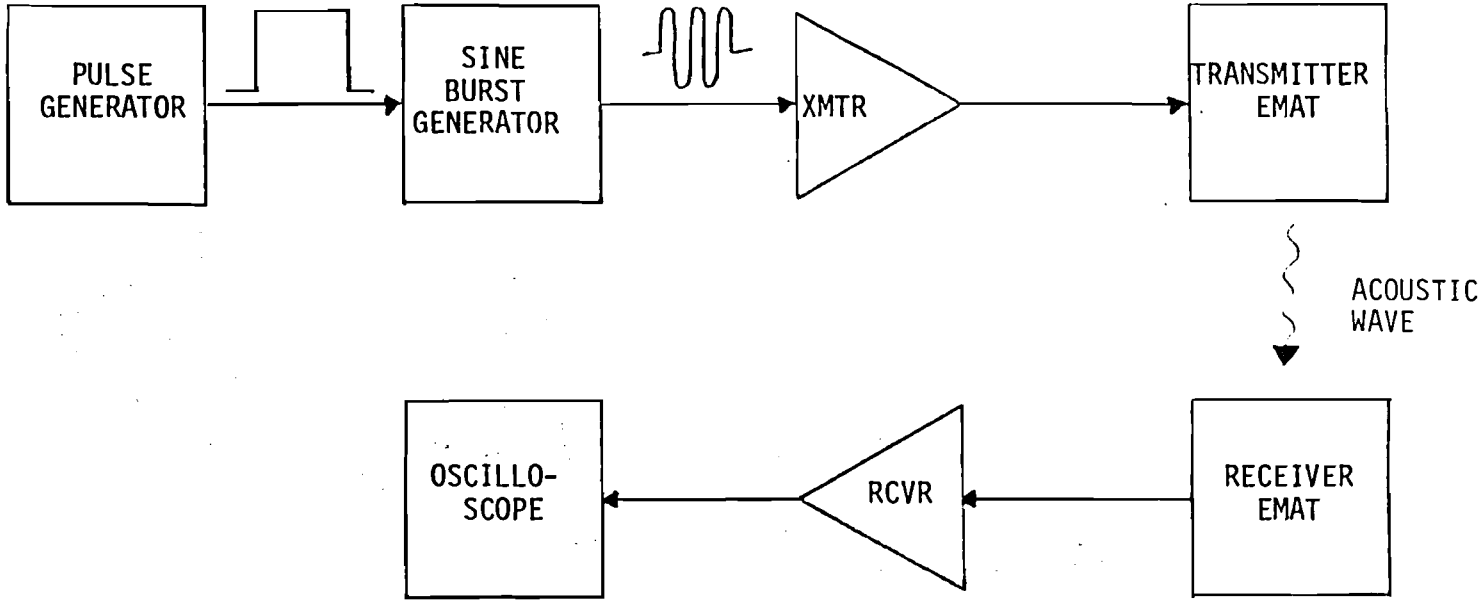

Fig. 15 Block diagram of the low frequency EMAT electronic system

Fig. 16 (a)
2 V/division
5 sec/division

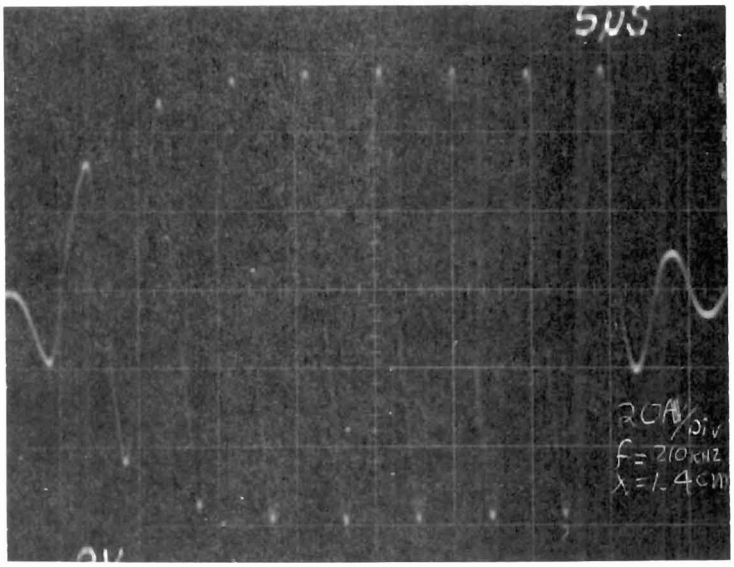

Fig. 16 (b)
1 V/division
50 sec/division

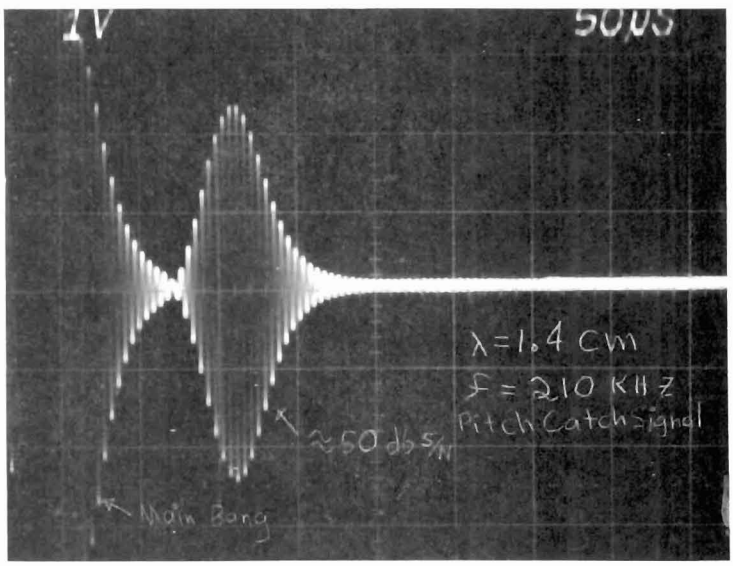

λ = 1.4 cm f = 220 KHz

Fig. 16 (a) RF burst of current delivered to the low frequency EMAT

Fig. 16 (b) Signal-to-noise ratio for the low frequency EMAT (approx. 50 dB) using pole piece No. 3, no EMAT lift-off, and ½" magnet lift-off

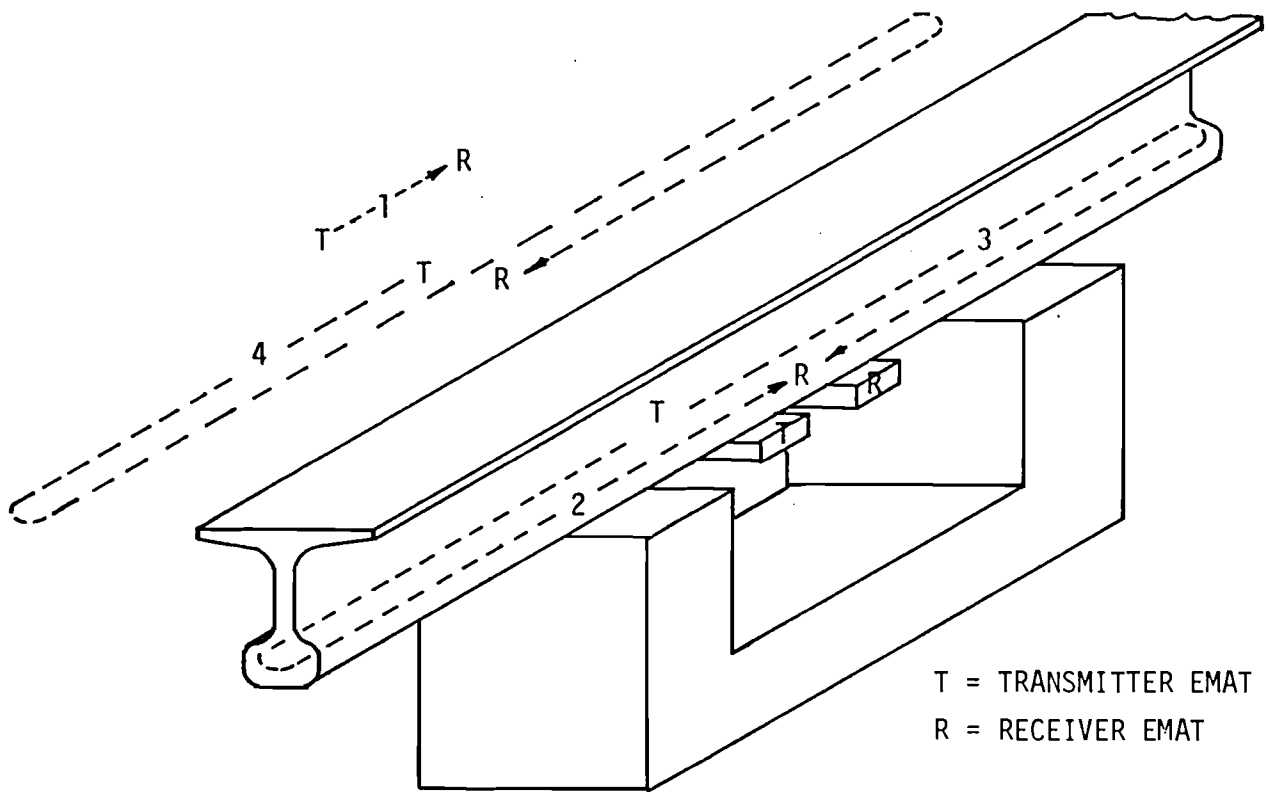

Fig. 17 Acoustic signal paths that occur in a rail sample excited by EMAT located in a tangential field for the detection of head defects at low frequencies

Freq. = 220 KHz, λ = 1.4 cm

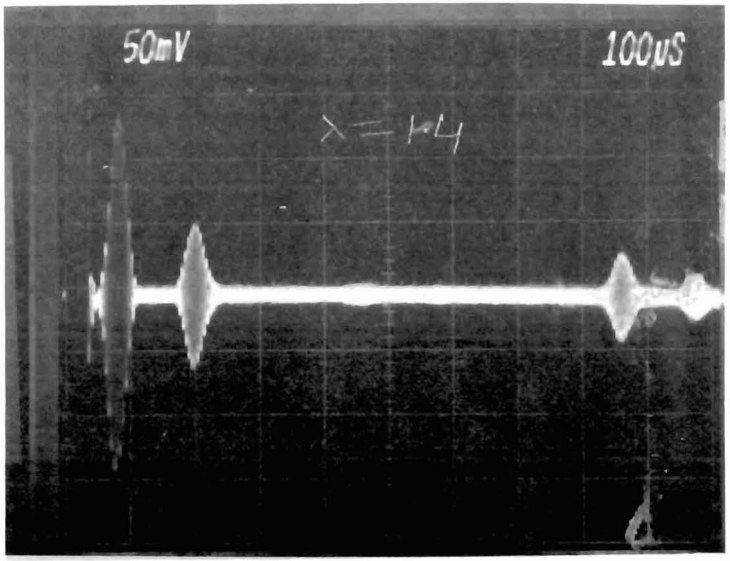

Freq. = 100 KHz, λ = 3 cm

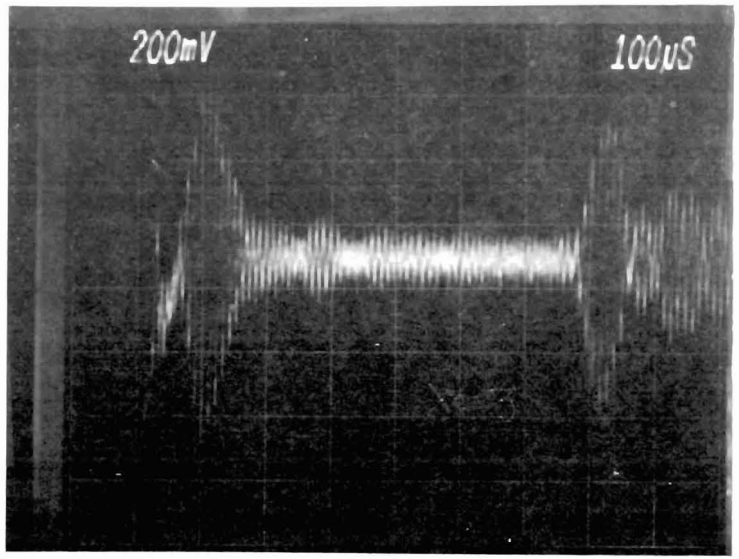

Fig. 18 Oscilloscope display of end reflection signals as described in Fig. 17.

(1) Direct transmitted signal

(2) Transmitter to left end of rail and back to receiver

(3) Transmitter to right end of rail and back

(4) Transmitter to left and then right end and back (direct transmitted signal is lost in the main bang for the 100 KHz case)

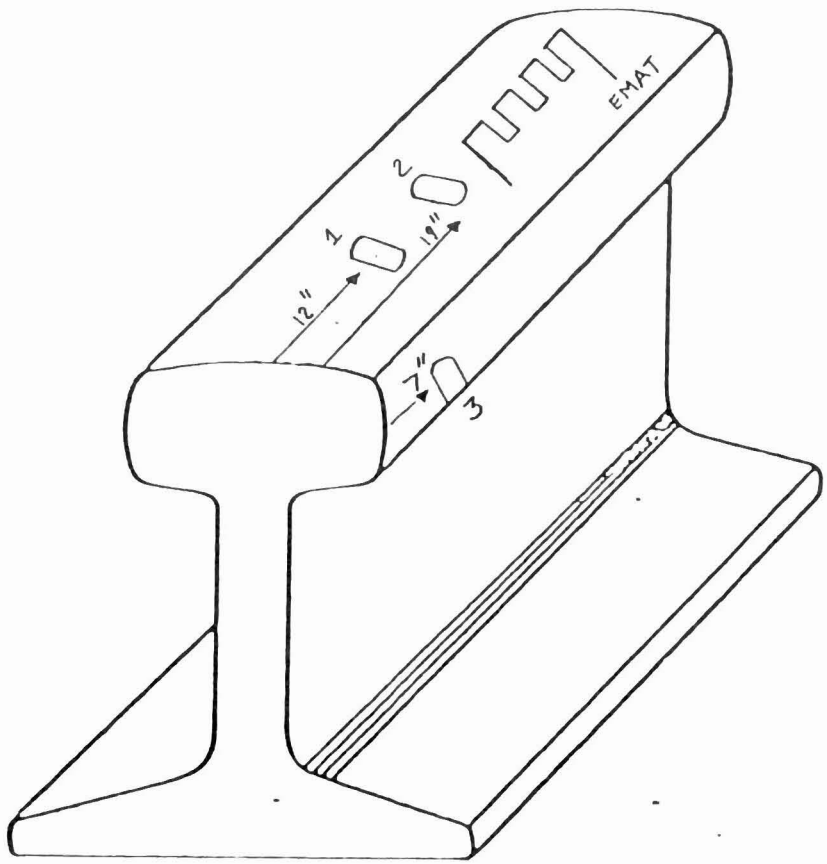

Fig. 19 Arrangement of 220 KHz EMATs and simulated flaws in an unflawed rail sample. Slots are approximately 1/8" wide, 1/2" long, and 1/4" deep.

100 μsec/div., 500 mV/div.

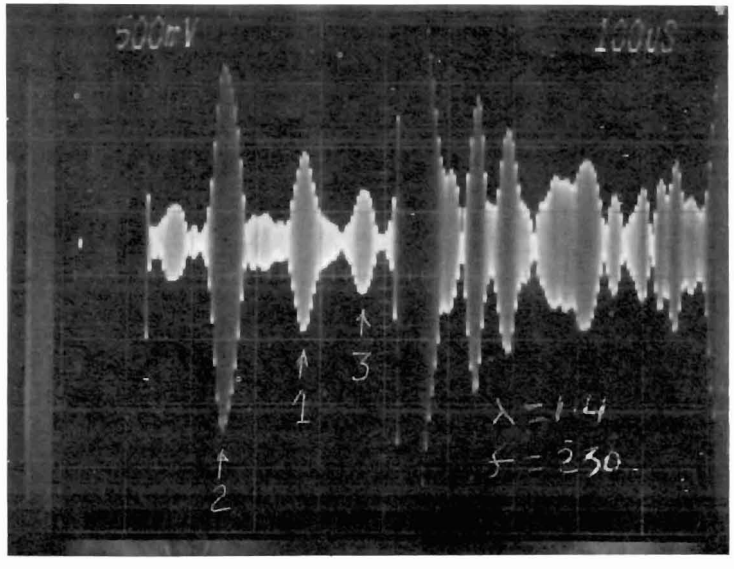

(a)

100 μsec/div., 500 mV/div.

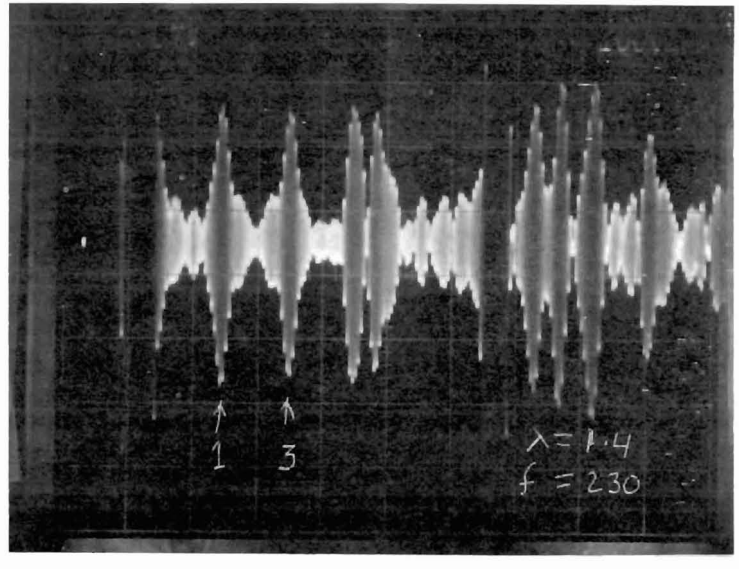

(b)

Fig. 20 Oscilloscope displays observed for reflections from the simulated defects in Fig. 19 using pole piece No. 1, 220 KHz, and λ = 1.4 cm. (a) EMATs positioned to show all three slots. (b) EMATs positioned so that slot #2 is merged in the main bang.

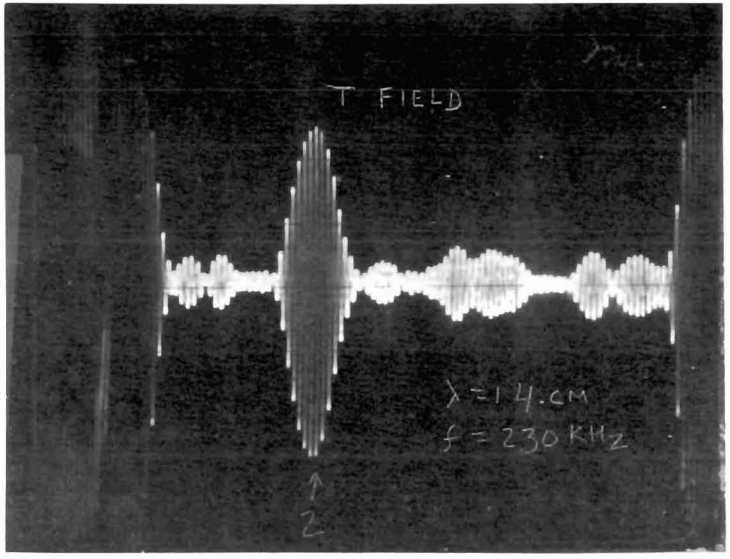

(a) Tangential Field

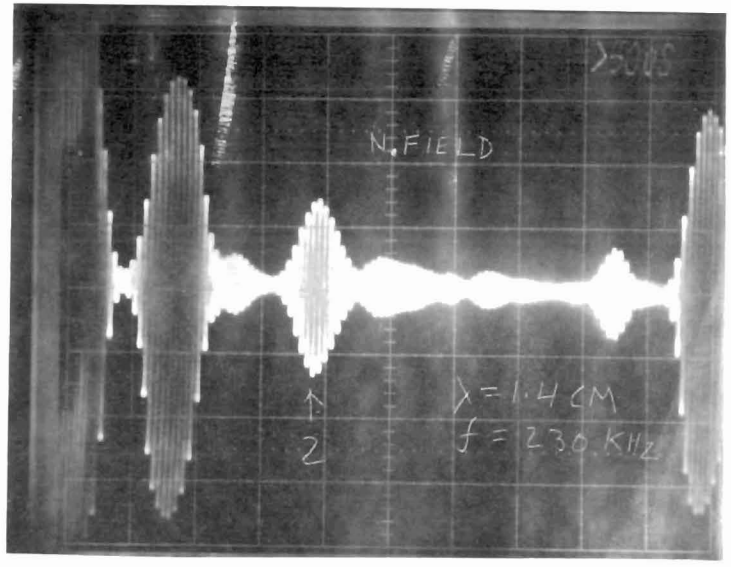

(b) Normal Field

Fig. 21 Demonstration of the defect detection sensitivity possible for the case of normal and tangential magnetic fields at the EMATs.

Note: See discussion on Page 13 on drawbacks of tangential field operation.

was positioned to produce an isolated reflection signal on the oscilloscope. Both of these photographs were obtained using pole piece No. 2. Clearly, for this one rail sample, the tangential magnetic field yielded a better signal-to-noise ratio than the normal field. However, some rail samples exhibited nearly zero coupling to the EMAT in a tangential field; thus, we conclude this field orientation is unreliable for the general inspection of rails in the field. Furthermore, by careful design of the pole pices and electromagnetic assembly, the normal flux can be concentrated to a point where the signal-to-noise ratio would be completely adequate to locate and identify critical flaws (such as those samples supplied) in in-service rail inspection.

To determine the acoustic reflection signals generated by actual flaws, the rails containing flaws as described in Tables I and II were mounted in the motion simulation device shown in Fig. 11 with EMATs in the normal field under the electromagnet pole pieces (the frequency was tuned to 220 KHz and an EMAT with a wave length of 1.4 cm was used). Figure 22 shows the electronic noise level in a well-tuned receiver channel on a 5 mv/div. scale to establish the signal level for a minimum detectable echo signal. We concluded from this picture that the electronic noise in the system was approximately 3 or 4 millivolts peak to peak. Figure 23 shows the acoustic signals observed in rail No. 6 which contained a horizontal split head. Signals 1, 4, and 5 arise from reflections from the left and right end of the rail, while signals 2 and 3 are reflections from the flaw. (Signal 3 is smaller than 2 because it results from reaching the receiver after an extra reflection from the end of the rail.) Note that there are signals between the echoes amounting to 300 mv peak to peak arising from small acoustic reflections (inhomogeneities) distributed throughout the rail. In most rails, it is this background of acoustic noise that sets the actual minimum detectable flaw signal rather than the receiver electronic noise (the same noise mechanism is present in piezoelectric inspections). Even in the presence of these spurious signals, the horizontal split head defects can be detected with a substantial signal-to-noise level by our low frequency EMAT system.

Rail sample No. 308 containing two transverse, detailed fissures produced the acoustic echo pattern shown in Fig. 24. The reflections from the two defects, labeled 1 and 2 in Fig. 24 (a), stand out clearly above the acoustic clutter signals. Figure 24 (b) shows defect signal No. 1 after improving the apparatus by using a more sharply tuned receiver and using the flux-focusing pole piece No. 3. Both photographs show a 6 to 1 signal-to-noise ratio, but the improved system shows less electronic noise. Similar data on detailed, transverse fissures are shown in Fig. 25 for rail No. 304 and in Fig. 26 for rail No. 306.

Figure 27 shows the echo received from the head inclusion specimen. Sperry identified this specimen as a head inclusion, which means a defective weld or an inclusion of foreign matter within the weld. The specimen

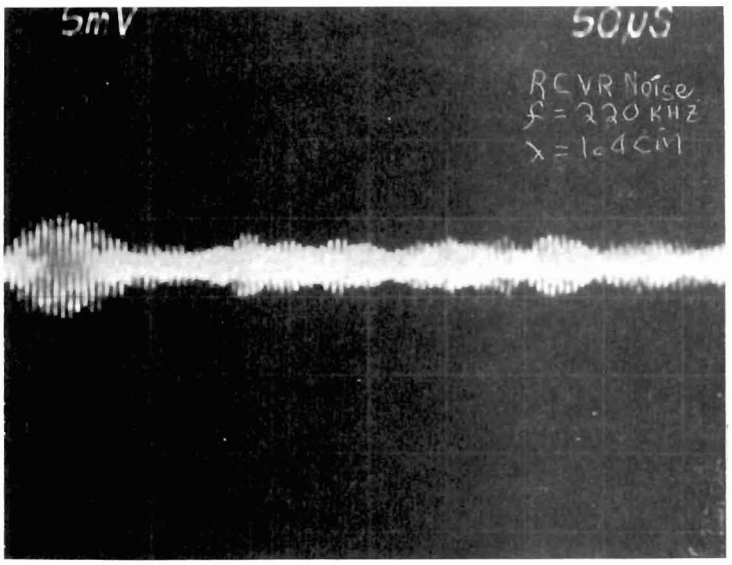

Fig. 22 Electronic noise level in the low frequency EMAT receiver channel at 220 KHz, wave length 1.4 cm., using pole piece No. 3.

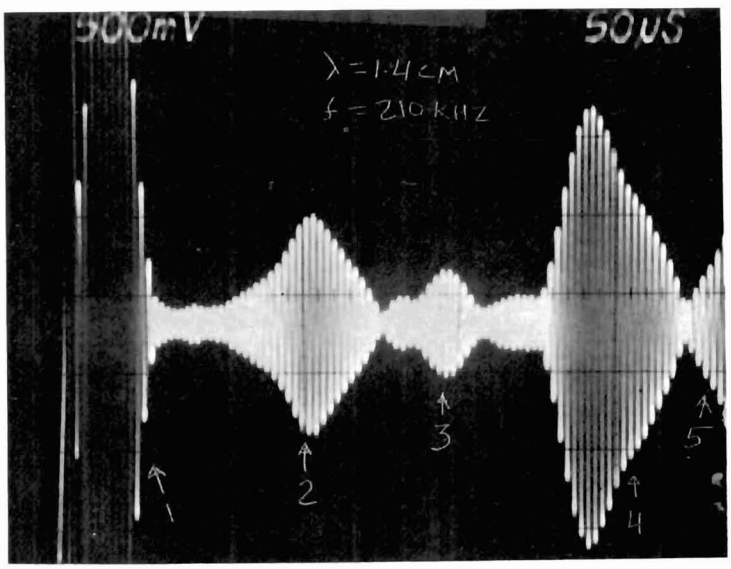

Fig. 23 Echo signals observed in rail No. 6 containing a horizontal split head. Signal 1 is the reflection from the nearby right-hand end of the rail. Signal 4 is the refelction from the far left end of the rail. Signal 2 is the signal reflected from the flaw, and signal 3 has been reflected from the flaw and from the right-hand end of the rail (freq. = 220 KHz, λ = 1.4 cm).

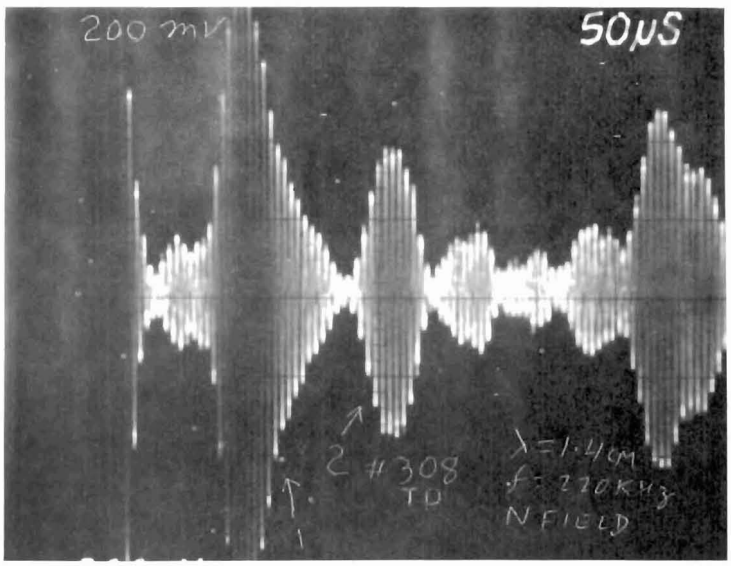

(a)

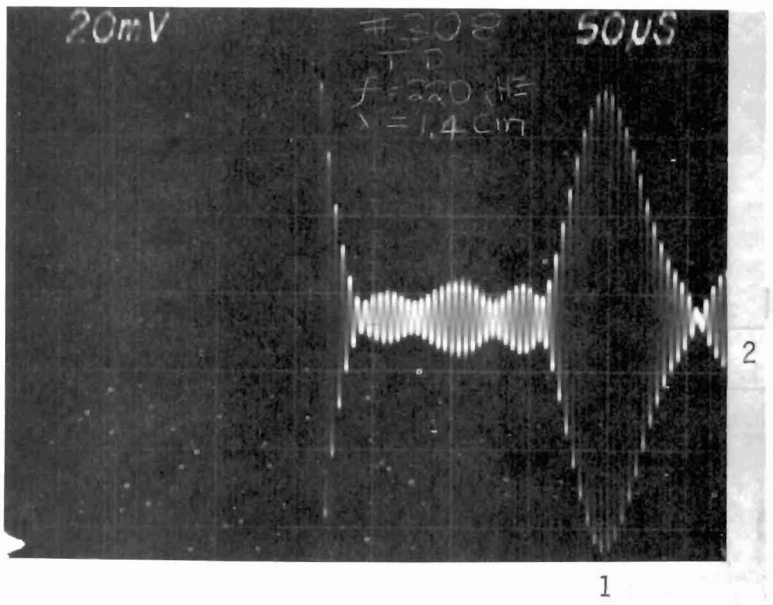

(b)

Fig. 24 Echoes from two transverse fissures in rail No. 308 (labelled 1 and 2). (a) Obtained with pole piece No. 2 and a wide band receiver. (b) Obtained with pole piece No. 3 and a narrow band receiver. (freq. = 220 KHz, λ = 1.4 cm)

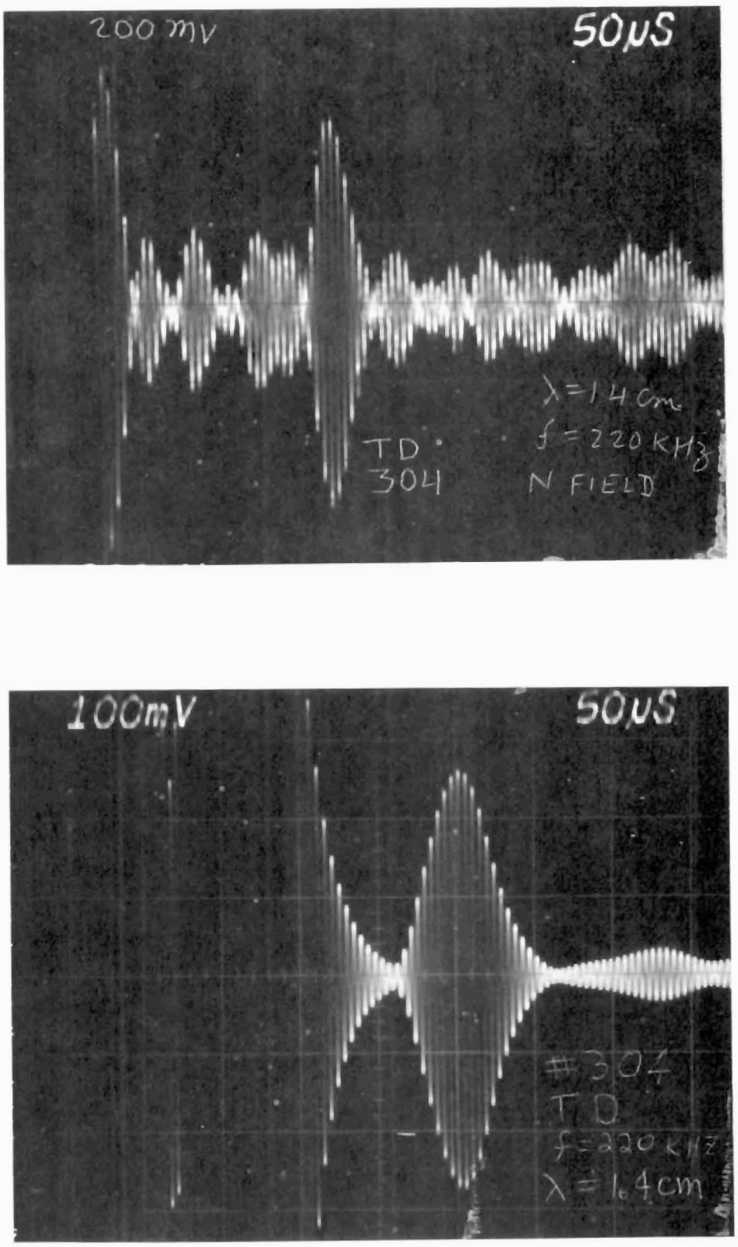

Fig. 25 Reflection from a transverse fissure in rail No. 304. The lower photograph is for an improved system in which a narrow band amplifier and pole piece No. 3 were used. The lift-off in the latter case was 1/16" and the normal field 12 Kgauss. (freq. = 220 KHz, λ = 1.4 cm)

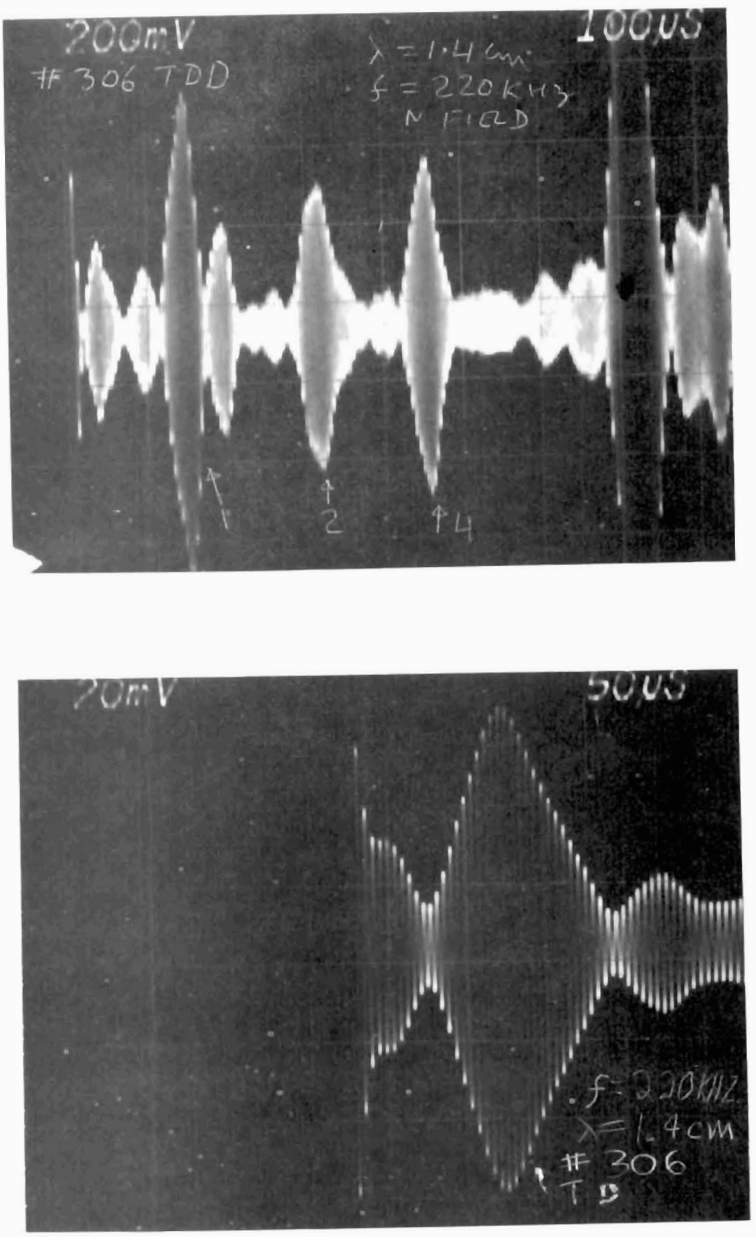

Fig. 26 Transverse defects 1, 2, and 3 observed in rail No. 306 using the wide band receiver and the improved system (bottom). (freq. = 220 KHz, λ = 1.4 cm)

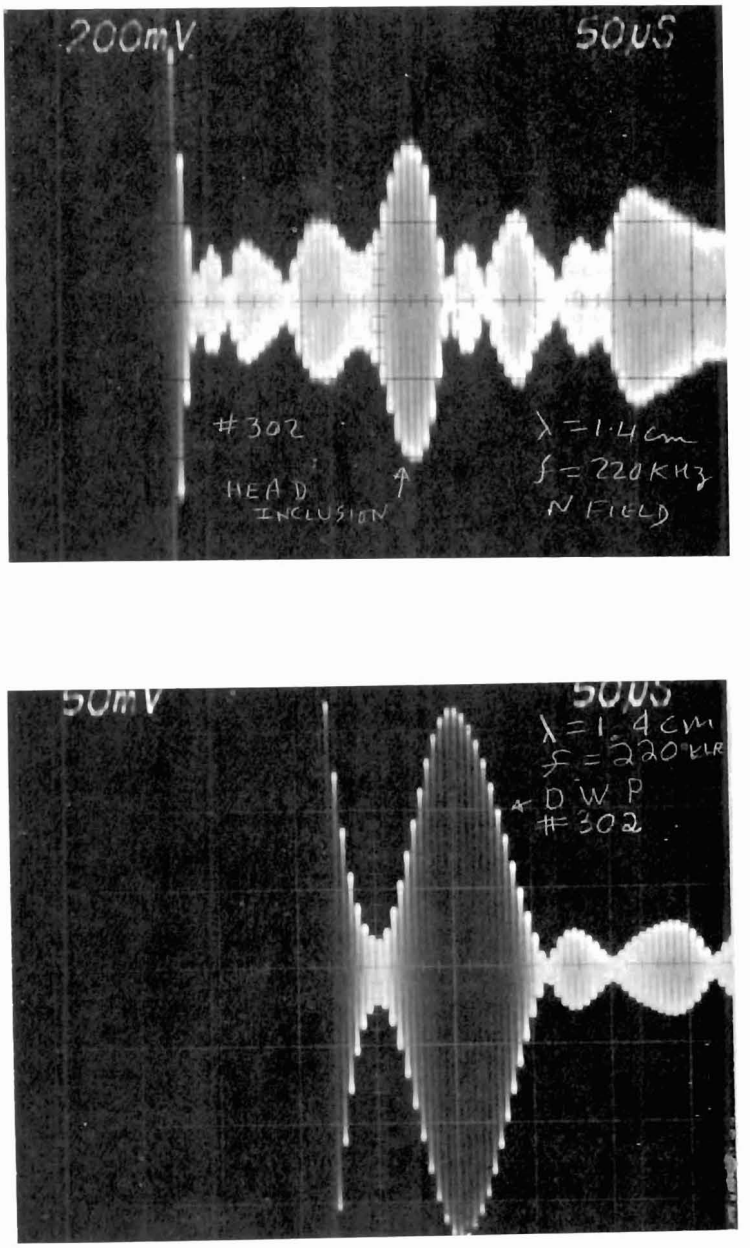

Fig. 27 Echo observed from an inclusion in the head of a welded rail. Rail No. 302, using the two electronic systems.

we have received also has a prominent weld bead with sharp edges on the underside of the head. The signals observed in Fig. 27 may be an echo due to the side defect, since the surface wave transducer is known to be sensitive to such surface flaws. At this time, we are not sure whether the echo observed with the low frequency EMAT has come from the inclusion or from the weld edge on the rail head.

Rails numbered 303 and 305 contain true transverse defects (T.D.T.) which do not intersect the surface. They could be detected by hand-held piezoelectric transducers launching 2.25 MHz ultrasonic waves into the head at an angle of 70 degrees relative to the head normal. They were not detected by the low frequency EMAT system when operating at 220 KHz, even after incorporation of the best receiver and pole piece. Presumably, this is because the 1.4 cm wave length waves launched by the EMAT did not penetrate the interior of the rail head but acted like surface or Rayleigh waves that are less sensitive to totally internal flaws. Certainly, many of the echo signals detected by the 1.4 cm wave system could be traced to surface irregularities--sometimes on the sides or bottom of the rail head. Additional experiments using flat bottom holes drilled into the end of the rail need to be carried out to verify this surface wave concept. As discussed in the next section, EMATs can launch and detect acoustic waves at a steep angle to the rail head normal direction so they conceptually can be designed to generate the same 70 degree angle beam that is used for piezoelectric flaw detection, and therefore should be capable of detecting the T.D.T. defect. Additional effort to determine the properties and sensitivity of 70 degree EMATs is suggested for the next program phase.

Two conditions that involve surface cracks that were experimentally detected by the low frequency EMAT system are the engine burn fracture (EBF) available in rail No. 309 and the surface shelling condition available in rail No. 307. Figure 28 shows the echo observed from the engine burn fracture near one end of rail No. 309. Here the flaw echo can be just resolved from the end reflection if very narrow acoustic pulses are used. For broader pulsed signals, the end reflection and the defect reflection become superimposed and interference effects occur. Surface shelling produces a collection of closely spaced echo signals as shown in Fig. 29. Each numbered echo is a reflection from a single shelling crack and the different displays seen in Fig. 29 were obtained by moving the rail so that the EMATs launched and detected waves from different locations along the rail. Since surface waves are sensitive to both EBF and shelling, it is difficult at present to differentiate between them. Deeply penetrating flaws, however, should be seen by the mid-frequency unit.

In all of these low frequency EMAT studies, the motivation was to find the lowest possible frequency at which all of the important flaws could be readily detected so that good lift-off performance could be anticipated. The previous results (Figs. 23 through 29) show that at 220 KHz and with a wave length λ = 1.4 cm, all the surface intersecting cracks produced easily observed reflection signals. Lower frequencies such as 110 KHz (λ = 3 cm)

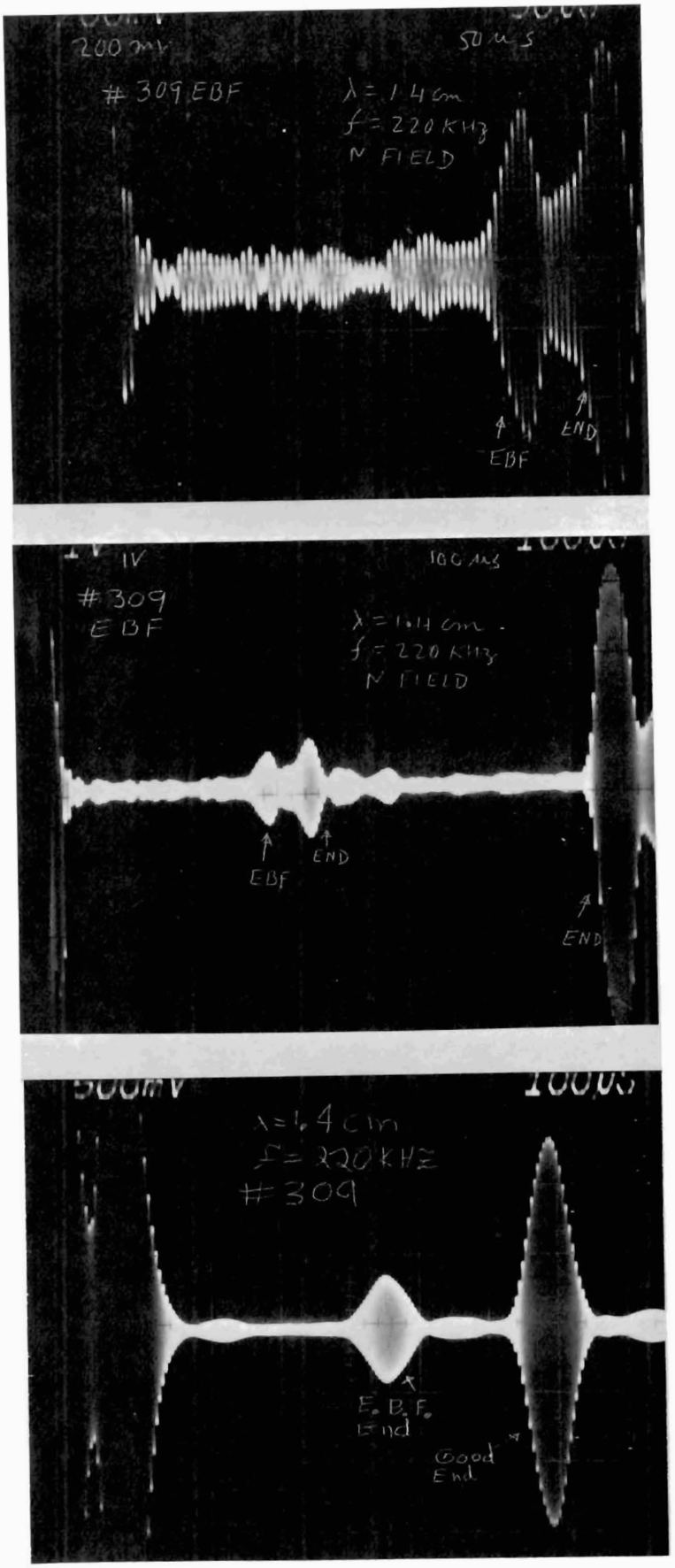

Fig. 28 Echoes observed from an engine burn fracture near one end of rail No. 309. (a) and (b) observed for short time duration signals. (c) observed when long time duration signals overlap and interfere. (freq. = 220 KHz, λ = 1.4 cm)

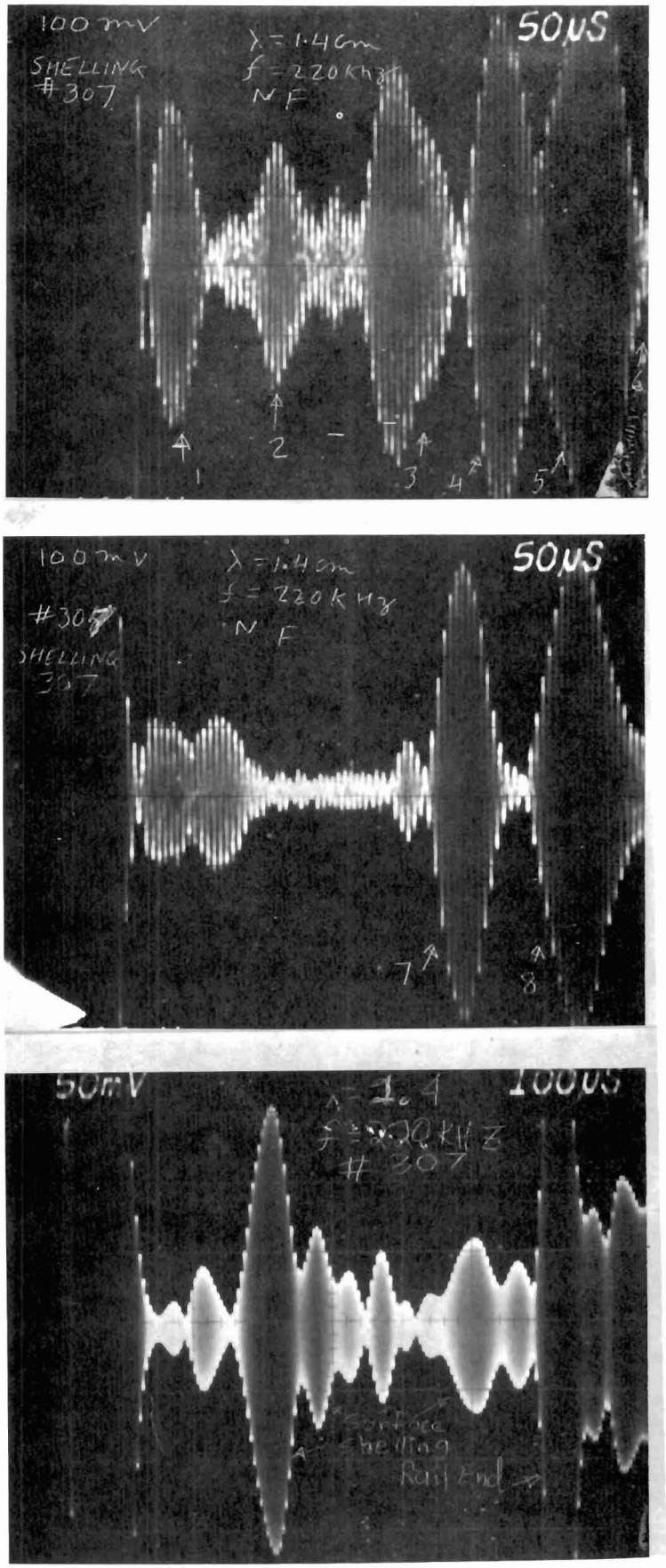

Fig. 29 Multiple reflections observed on rail No. 307 caused by surface shelling. (freq. = 220 KHz, λ = 1.4 cm)

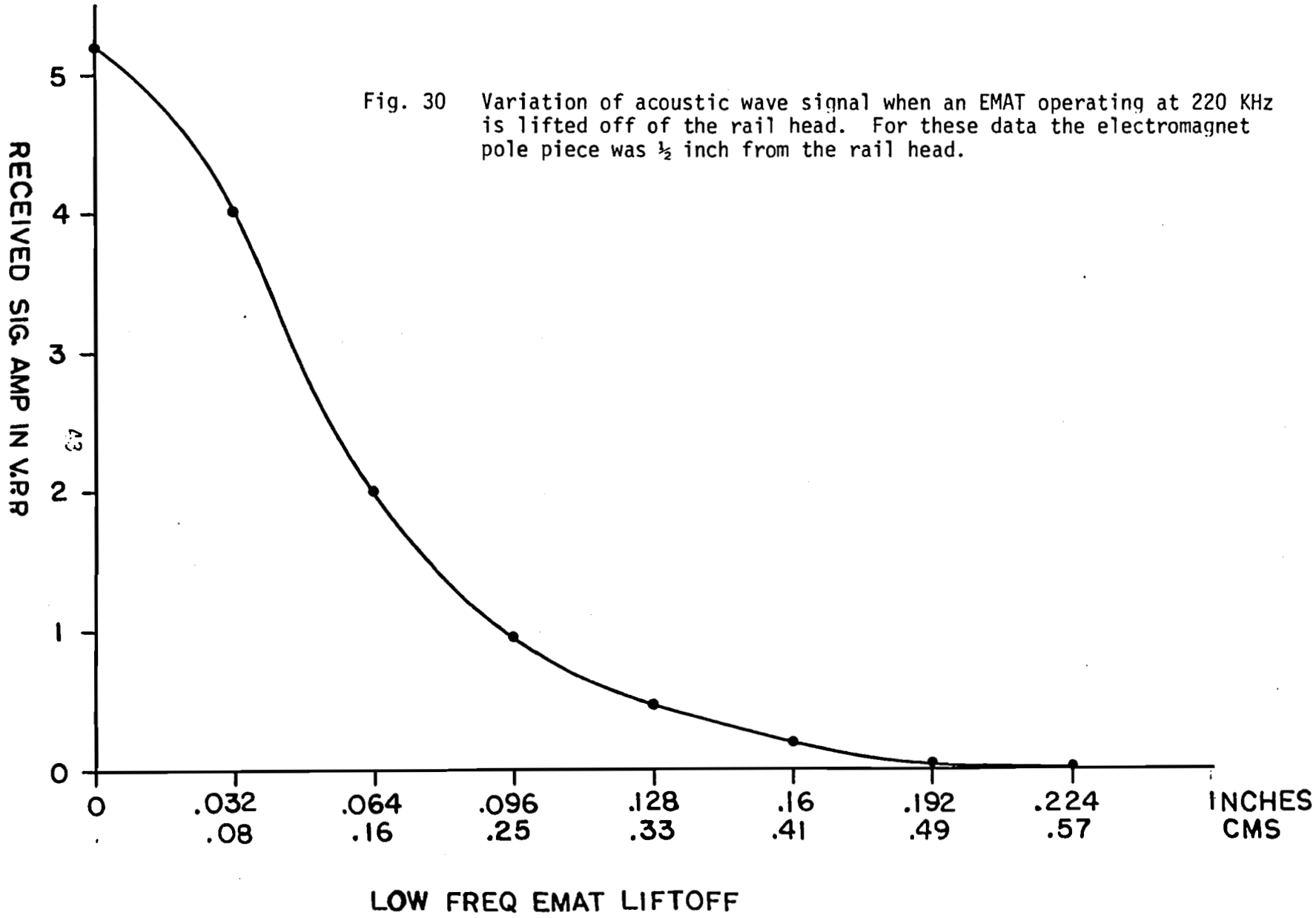

Fig. 30 Variation of acoustic wave signal when an EMAT operating at 220 KHz is lifted off of the rail head. For these data the electromagnet pole piece was ½ inch from the rail head.

were also studied, but the echoes at this frequency were poor because they had a long time duration. Higher frequency waves were not useful because the short wave lengths would not penetrate deeply into the rail head. Hence, a frequency of 220 KHz and a wave length of 1.4 cm appeared to be the optimal choice for detection of rail head defects. The lift-off characteristic of an EMAT operating at this frequency is shown in Fig. 30. It can be seen that beyond 1/16 inch separation between the rail and the EMAT coils, the acoustic wave signals fall to an uncomfortably low level. However, it is anticipated that 1/16 inch separation would be practical for the light EMAT element in a realizable field rail inspection system.

B. Medium Frequency

The medium frequency EMAT design was chosen to have a wave length substantially smaller than the thickness of the web so that the ultrasonic waves could freely propagate into the web from the head without distortion. The width of the transducer was made wide enough to completely span the web and make transducer alignment uncritical. This led to a choice of frequency near 500 KHz and an approximately 1 cm wave length. Figure 31 shows how transmit-receive EMATs were positioned over the rail head in a normal magnetic field to inspect the web and bolt holes by an angle beam, pulse-echo method similar to that used in piezoelectric transducer inspection systems. Figure 13 in Section III shows the details of how the intermediate frequency EMAT was wound with the transmitter and receiver coils intermeshed to reduce the coupling between them and to occupy the small space available under pole piece No. 3. Figure 32 shows a block diagram of the circuit elements used for the medium frequency investigations.

As discussed in Section II, a formula is available which relates the frequency that the EMAT is driven to the angle at which the acoustic waves are radiated. This relationship was tested in a rail specimen by placing a transmitter on the head of the rail and a receiver on the base of the rail so that the line joining them made an angle θ relative to the rail head normal (as shown in insert of Fig. 33). At each frequency, plotted on the abscissa, the receiver was positioned for a maximum signal and the angle was measured. Figure 33 shows that the maximum acoustic emission occurs at an angle of between 30 and 45 degrees. That is, there is a maximum in transduction efficiency when the acoustic waves were radiated at an angle of 30 to 45 degrees from the rail head normal at these frequencies. Figure 34 compares the theoretical relationship to the measured data for frequency versus angle of acoustic emission. These patterns are in adequate agreement with the observations.

It was also of interest to examine the distribution of acoustic energy (beam width) produced by an EMAT operating in the angle beam mode. This was done with the same transducer arrangement as shown in the insert of Fig. 33, except that the transmitter and receiver had an interwire spacing D = 0.7 cm (λ = 1.4 cm) 4 loops and they were operated at a frequency of 400 KHz.

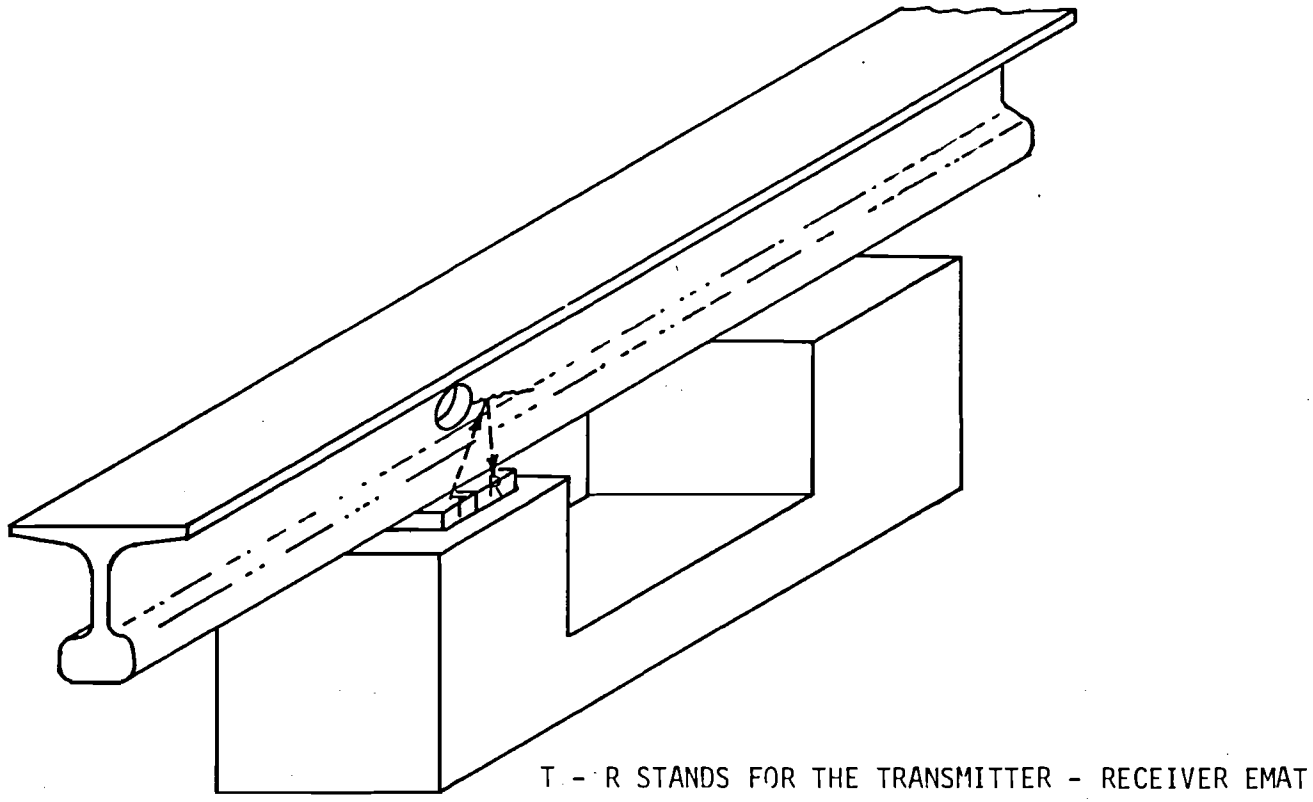

Fig. 31 Detection of web defects using a medium frequency EMAT in a pitch-catch mode

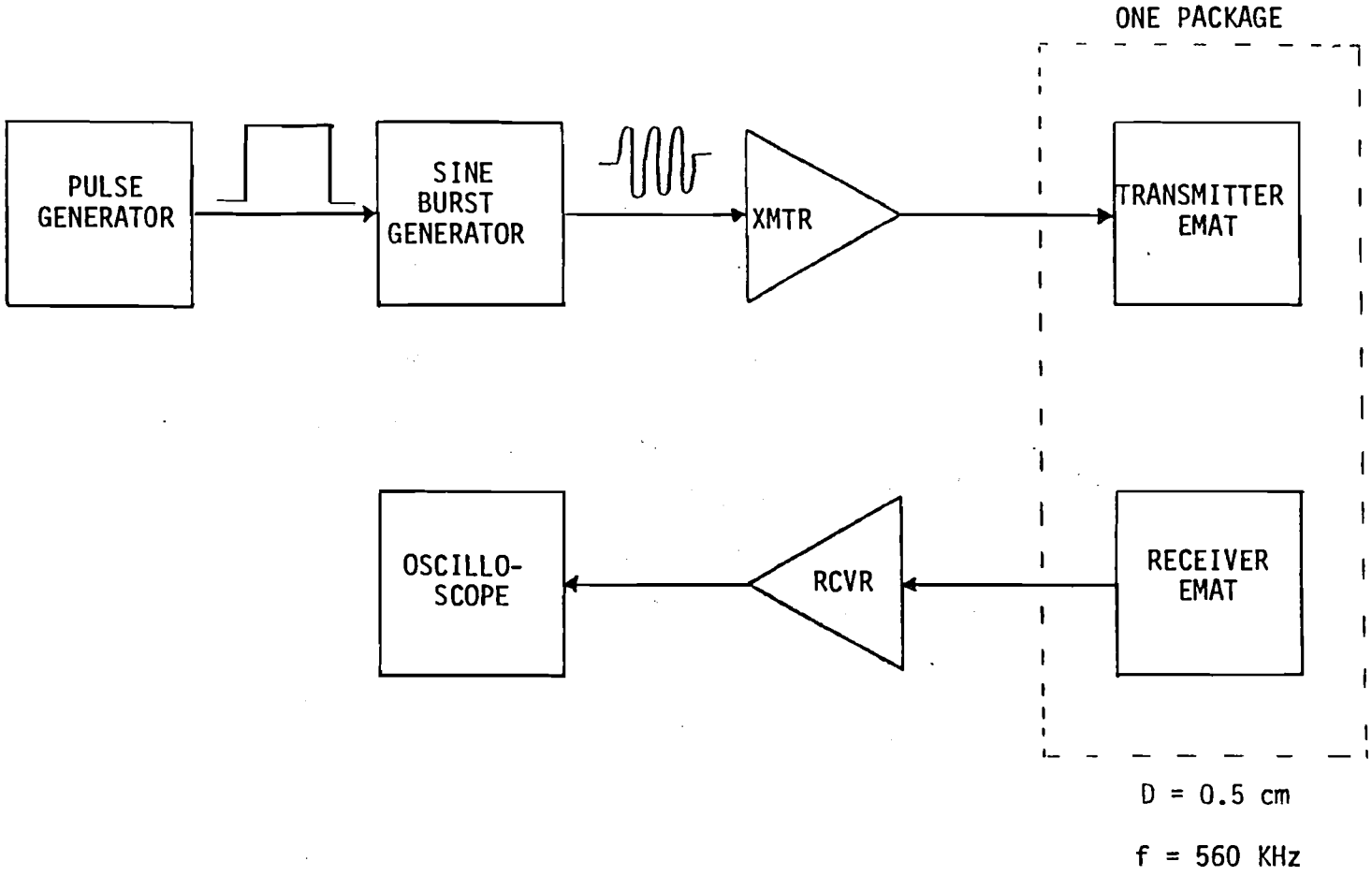

Fig. 32 Block diagram of the mid frequency EMAT system

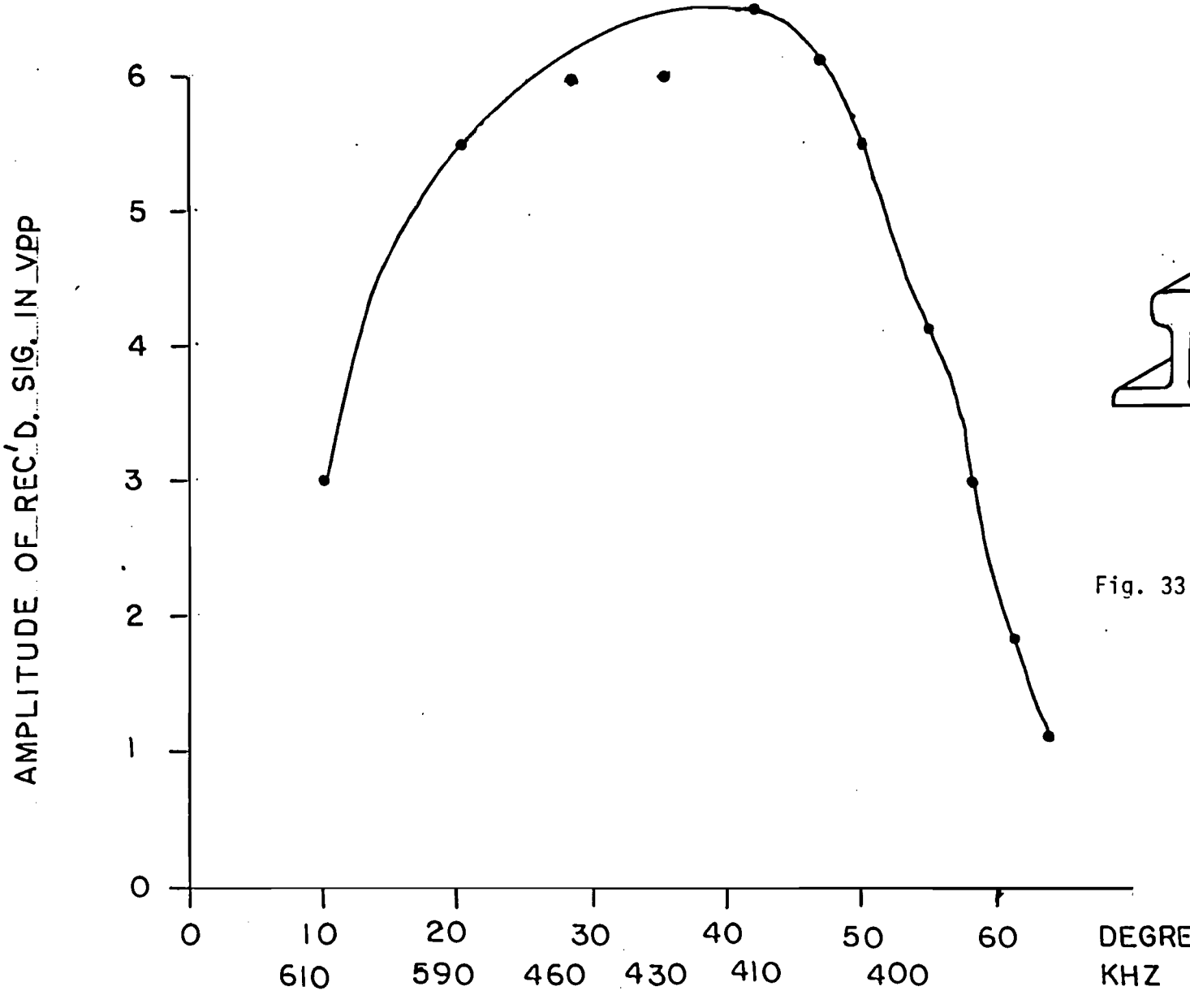

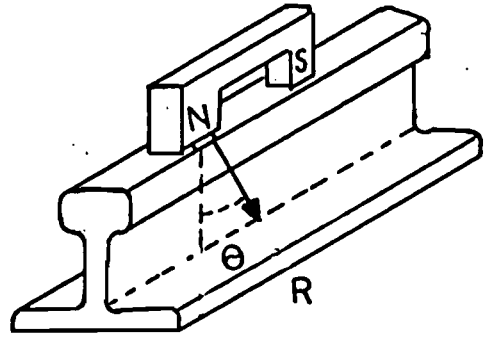

Fig. 33 Observed signal strength of received signal for different frequencies and corresponding angles θ observed.

$$\theta = \sin^{-1} \frac{Vs}{2fD}$$

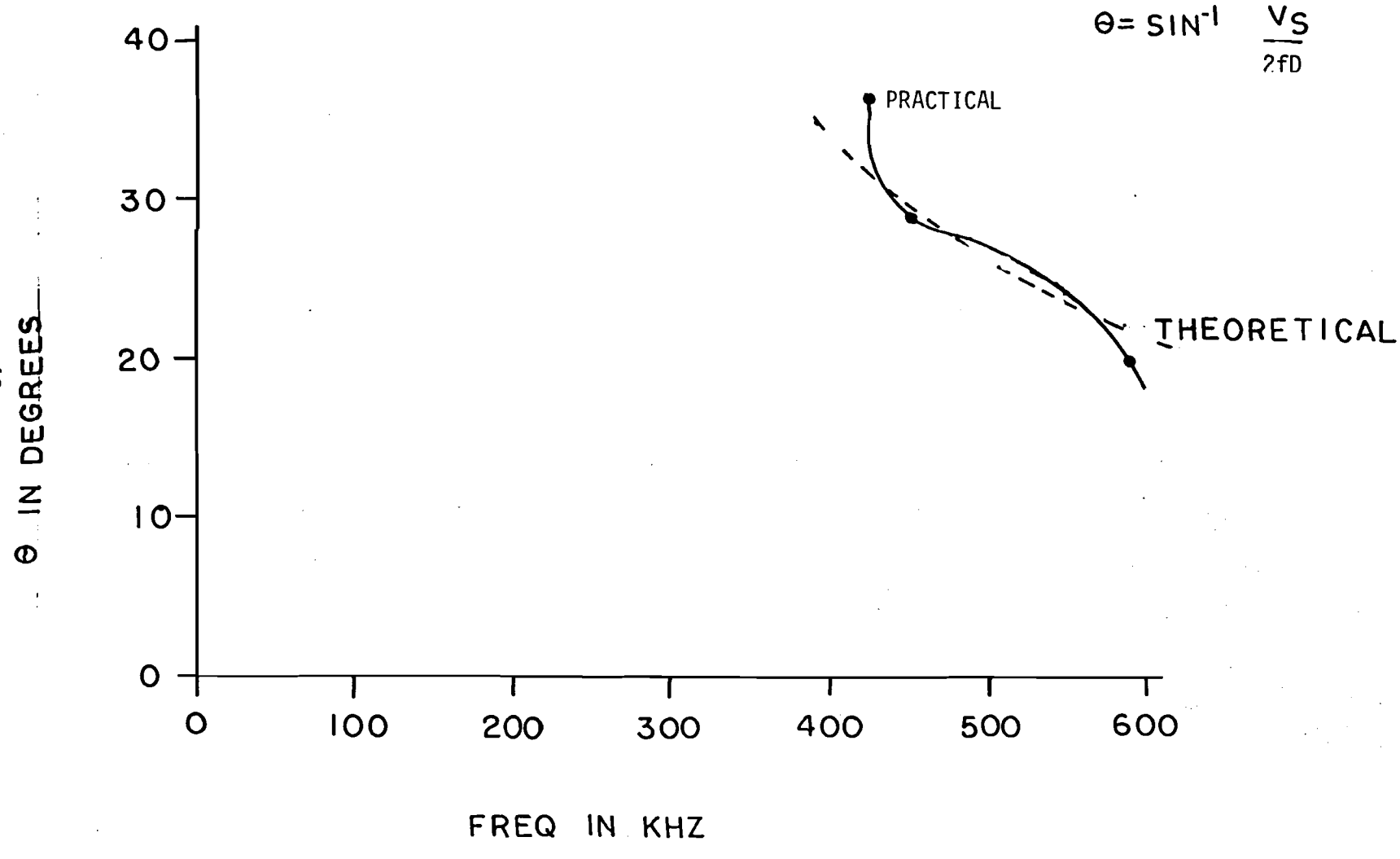

Fig. 34 Comparison between the theory and experiment for the angle of radiation by an EMAT driven at various frequencies.

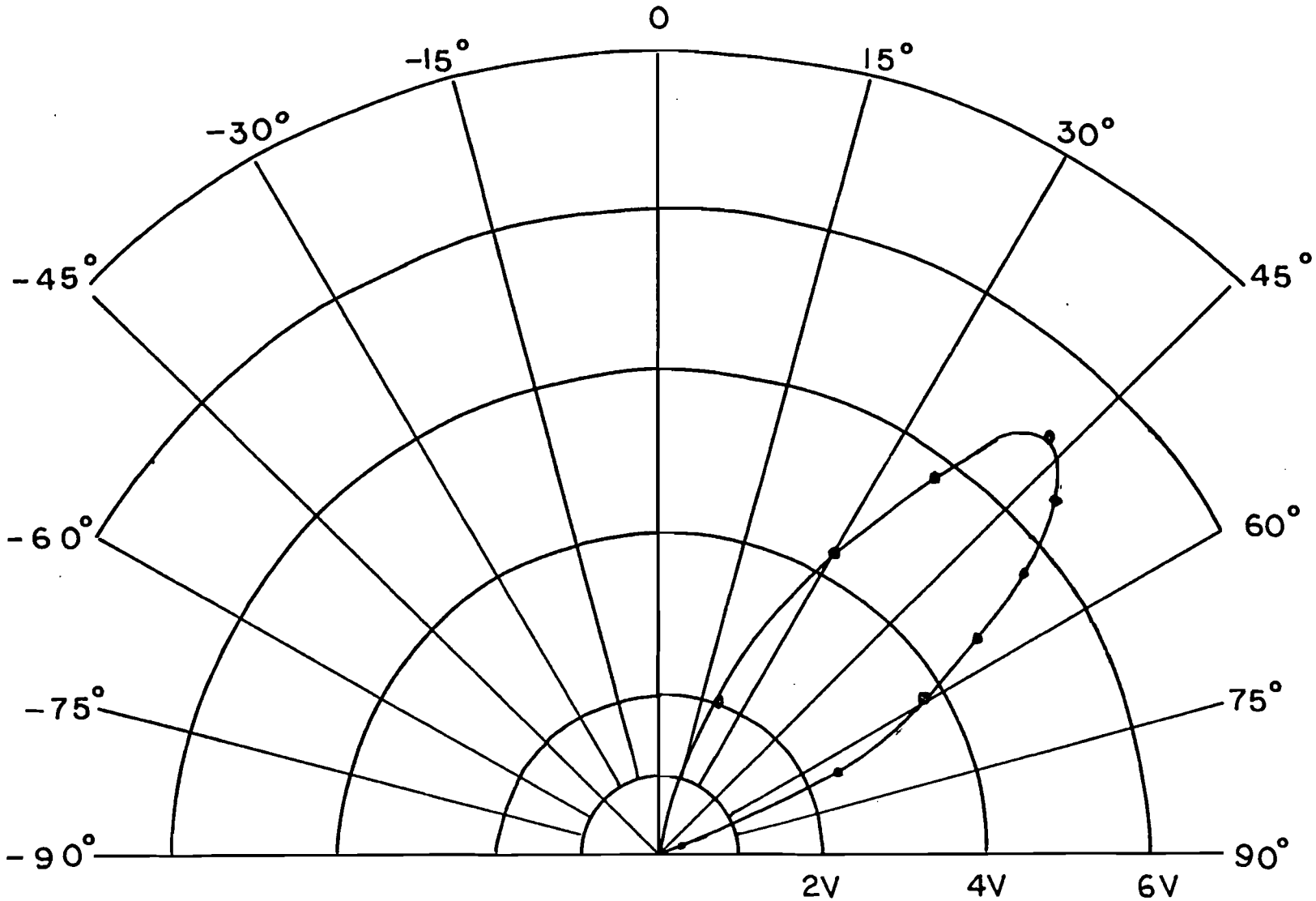

Fig. 35 Angular dependence of the acoustic energy radiated from a meander coil EMAT with wire spacing ½ cm driven at a frequency of 400 KHz.

Figure 35 shows the observed angular distribution of acoustic energy reaching the base of the rail plotted on polar coordinates. The observed angle of maximum radiation ($\sim 42°$) is slightly larger than that predicted by Eqn. 2 (of 35°). One explanation is that the detailed interaction of the eddy currents and the magnetic field superimposes an additional angular dependence that causes the combined efficiency to peak at slightly larger angles. Independent of these quantitative details, Fig. 35 demonstrates that an EMAT can successfully launch angle beam shear waves into the web of the rail without serious distortions in the beam pattern.

For most of the detailed rail measurements made with the medium frequency test unit, a transducer with a wire spacing of 0.5 cm (λ = 1 cm) was operated at a frequency of 560 KHz using the optimized electromagnet pole piece No. 3. Figure 36(a) shows an oscilloscope display of the current RF burst delivered by the transmitter to the EMAT. The acoustic signal reflected from the base of the rail is shown in Figure 36(b) when the receiver was separated from the transmitter. Note that the signal reaching the receiver after propagating through the head and web is still well shaped (no dispersion or extraneous reflections) and exhibits a 40 dB signal-to-noise level. In a practical inspection system, the existence of a reflection from the base could be used to indicate the absence of any flaws in the web which tend to shadow or scatter acoustic energy from the flat rail base. Thus, the disappearance of the base reflection signal would indicate a head-to-web separation, a crack in the web, or a bolt hole. These conditions were observed in the laboratory and hence are a viable basis for flaw detection.

The detection of a bolt hole crack was considered to be such an important problem for the EMAT inspection system that two methods were developed to detect this problem. The first uses a pitch-catch mode, where the transmitter and receiver are separated (as described above), a flawless bolt hole blocks the reflection from the base over a well-defined distance while a cracked bolt hole is observed to make this distance larger than normal. This change in apparent dimensions of the bolt hole is now used by Sperry Rail Service as an indicator of bolt hole cracks and could be used in an EMAT inspection system. However, a more positive identification technique was developed using the integral transmitter/receiver EMAT (Fig. 13) in a pulse-echo mode. In this mode, no reflection signals are observed in a normal rail. When a bolt hole intercepts the beam, a large reflection signal similar to that shown in Fig. 37 could be observed when the alignment of the acoustic beam with the hole was very good. Since the acoustic beam used in the experiments was wide and illuminated more than one bolt hole at the end of a rail, the reflection from a flawless row of bolt holes was observed to show many maxima and minima as constructive and destructive interference between the reflections from adjacent holes as the EMAT was moved down the rail past the bolt holes. If one of the bolt holes contained a crack, the interference effects were drastically reduced or eliminated so that the reflection signal remained at a magnitude that was very

(a)

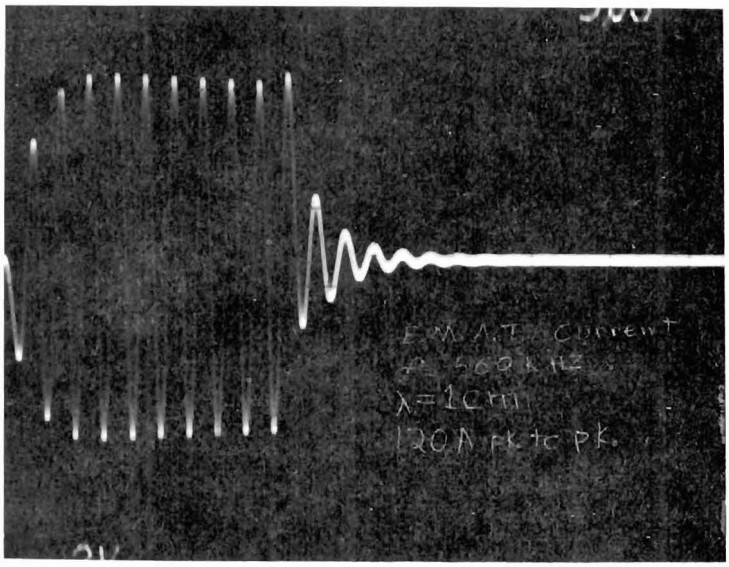

(b)

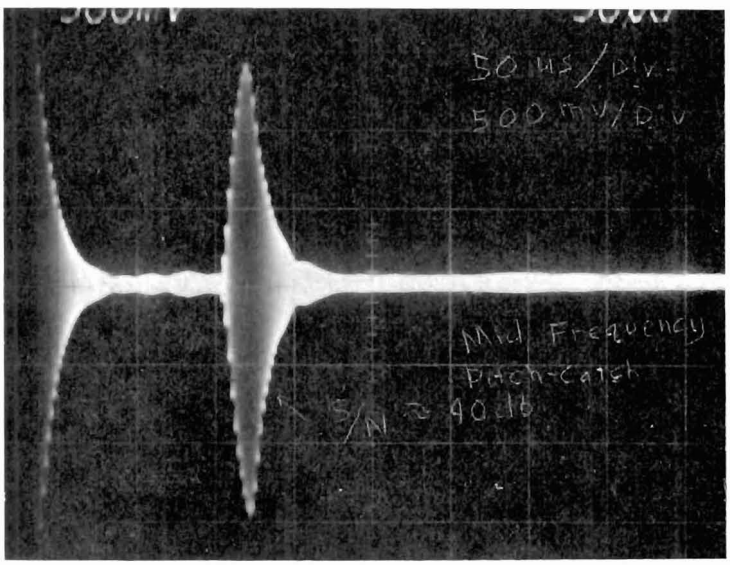

Fig. 36 Performance of the optimized, mid-frequency system. (a) Current waveform delivered to transmitter EMAT, 120 amps peak-to-peak. (b) Signal reflected from base of rail in a pitch-catch mode.

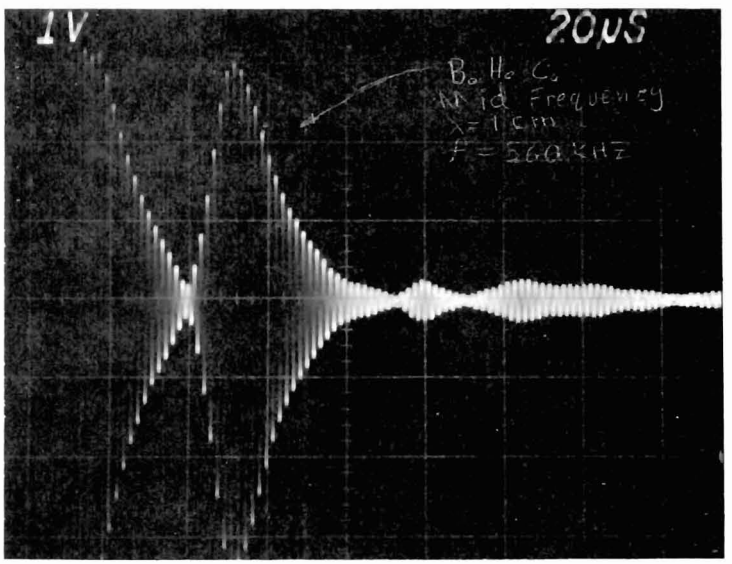

Fig. 37 Reflection observed from a bolt hole crack using a pitch-catch, angle beam EMAT system operated at 560 KHz and a 1 cm wave length.

large as the EMATs were translated past the holes. Figure 38 displays this phenomenon in a graphical sketch. It is anticipated that rather simple signal processing techniques could be used to distinguish between unflawed bolt holes and those that have a crack from one of the bolt holes. It can therefore be concluded that EMATs operating near 600 KHz in an angle beam mode are able to inspect the web of a rail for the most important classes of flaws.

Figure 39 shows the lift-off sensitivity of a mid frequency angle shear EMAT system. These data suggest that a system operating with between 1/32" and 1/16" lift-off should have adequate sensitivity and be amenable to field implementation.

C. High Frequency

Meander coil EMATs which operate at frequencies near 1 MHz were used in the original feasibility study for locating small defects in the head of the rail. Because of their small acoustic wave length, severe lift-off sensitivity precluded their straight-forward application. Thus, a meander coil based system would be very difficult to implement in a practical inspection system. In order to use EMATs to find small flaws in rails, a different design approach had to be considered. If the coil is wound as shown in Fig. 3, a bulk shear wave can be launched into the metal in a direction normal to the surface and the sensitivity to lift-off is minimized. Such a bulk wave would be analogous to the 0 degree piezoelectric transducer inspection now being carried out by current rail inspection services.

A flat EMAT coil, similar in shape to that shown in Fig. 3, was wound on a PC board 1/16" thick x 0.75" wide x 1.2" long. A sheet of 0.002" thick copper was placed under the windings which would be farthest from the rail head to shield the head from the currents on this side of the coil. This coil was used both as a transmitter and receiver EMAT, and a TR (transmit/receive) switch was placed in the circuit as shown in Fig. 40. The current RF burst fed to this EMAT was 50 amperes (p to p) and the noise level from the receiver was 70 millivolts (p to p). (See Figure 41.)

The results shown in Fig. 42 were obtained with the EMAT over an unflawed portion of rail, Fig. 42 (a), and over a bolt hole, Fig. 42 (b). Clearly, the presence of the bolt hole eliminates the large base reflection arriving at 120 μsec, and the disappearance of this signal over a measured travel distance could be used to distinguish between a flawless bolt hole and a cracked bolt hole. Note that the small signal arriving at 53 μsec, which is the reflection from the bottom of the rail head, is unchanged by the passage of the EMAT over a bolt hole.

The horizontal split head and the head and web separation defects are both easily detected by this high frequency, 0 degree shear acoustic beam EMAT,

(a)

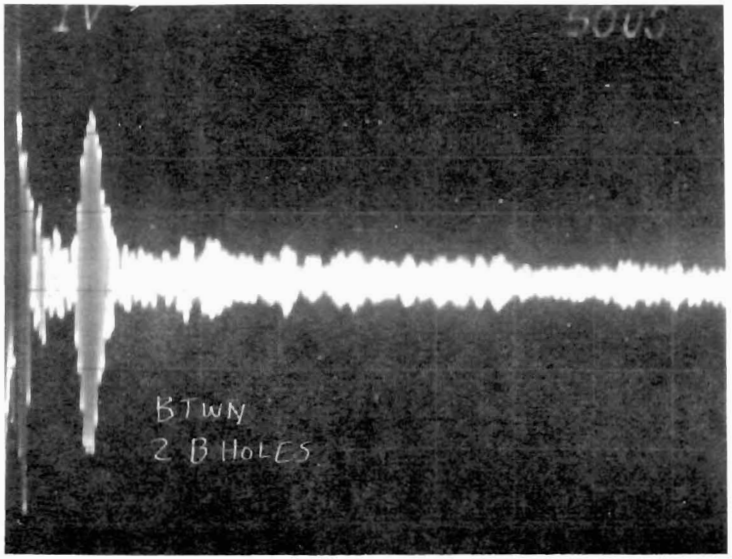

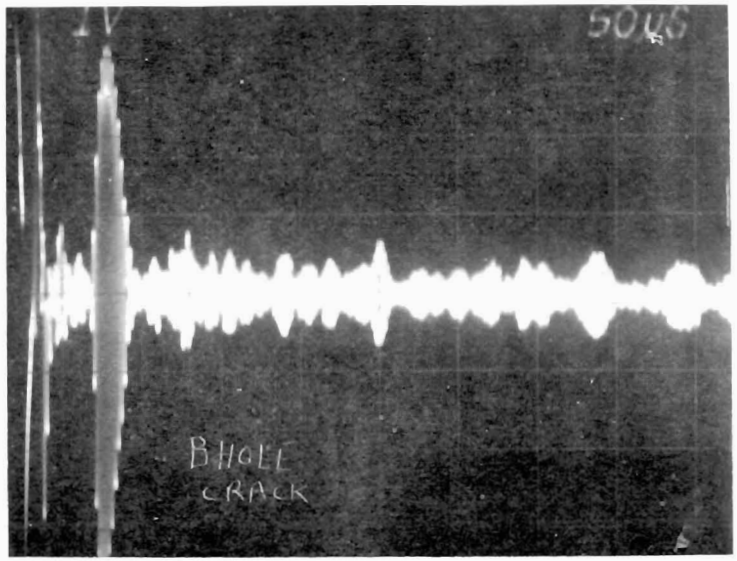

(b)

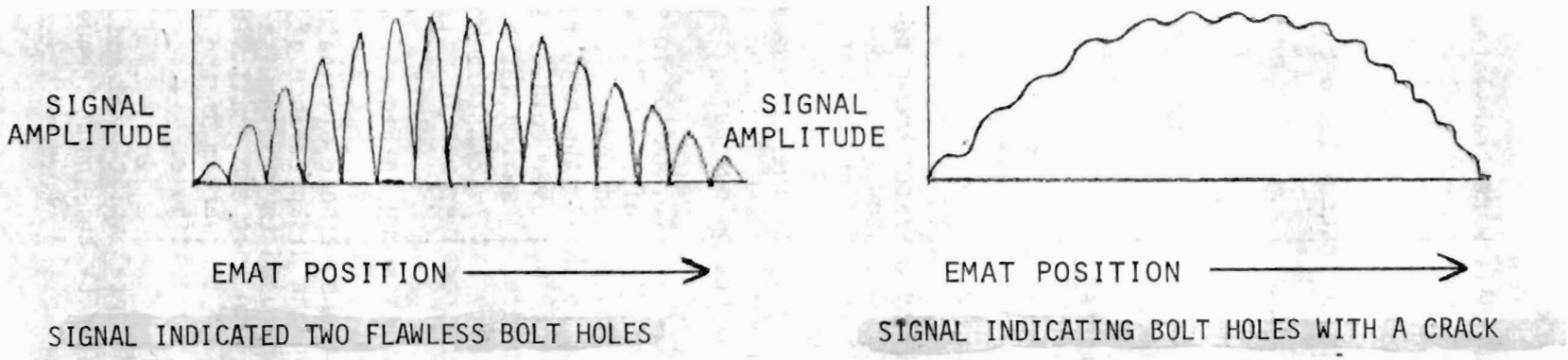

Fig. 38(a) Characteristics of pulse-echo signals observed in the vicinity of flawless bolt holes and cracked bolt holes for intermeshed EMATs operated at 560 KHz and λ = 1 cm with pole piece No. 2. The sketch, (b), plots the maximum reflection amplitude observed as a function of position as the EMAT is translated down the rail. The sharp nulls, characteristic of a unflawed series of bolt holes, are not present when a crack is present in one or more bolt holes.

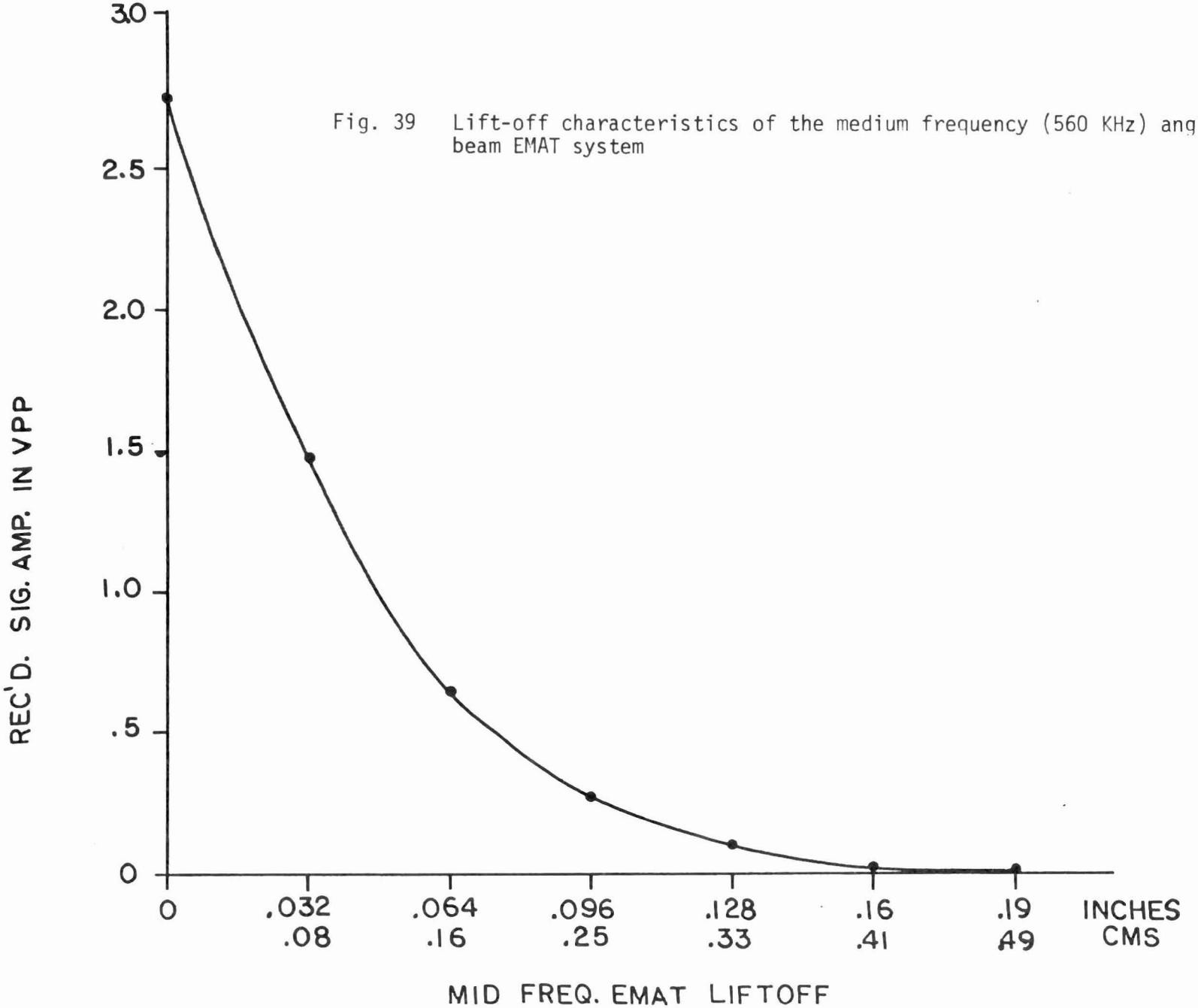

Fig. 39 Lift-off characteristics of the medium frequency (560 KHz) angle beam EMAT system

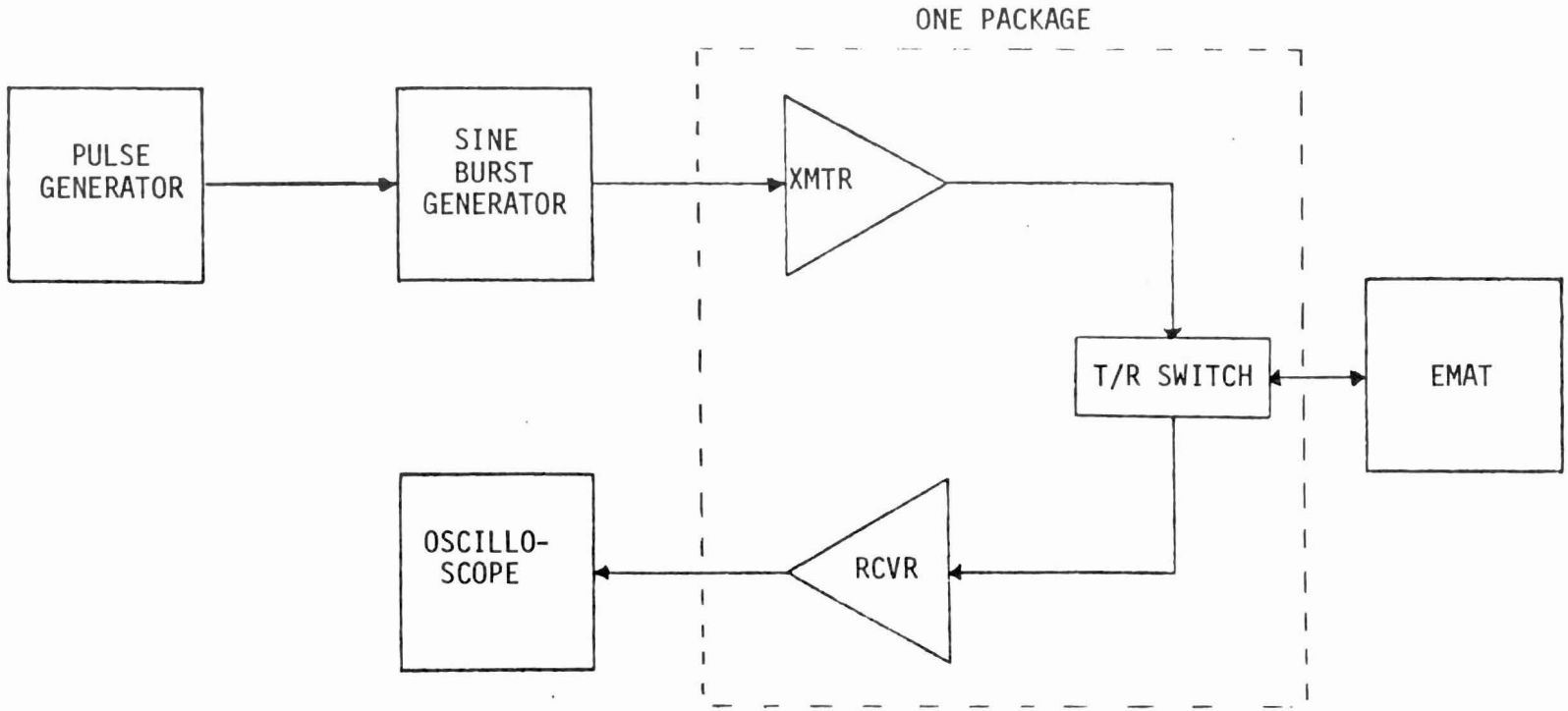

Fig. 40 Block diagram of the high frequency EMAT system which operated at a frequency of 2 MHz (λ = 0.16 cm).

(a)

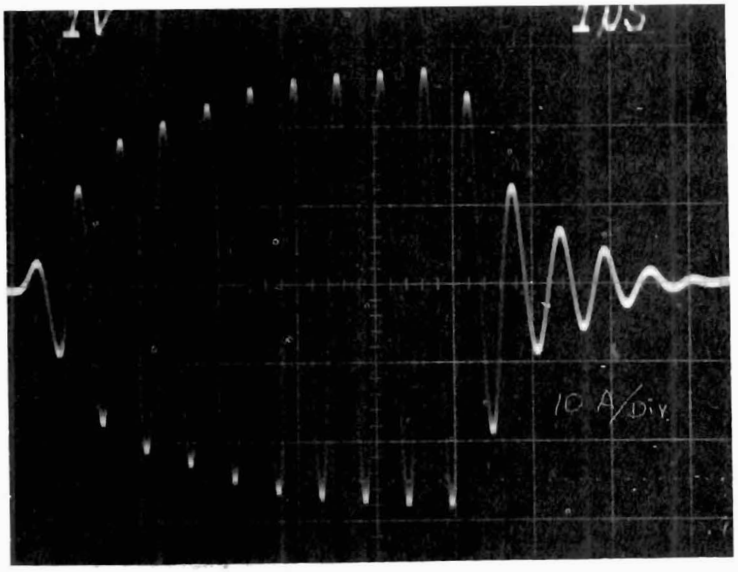

(b)

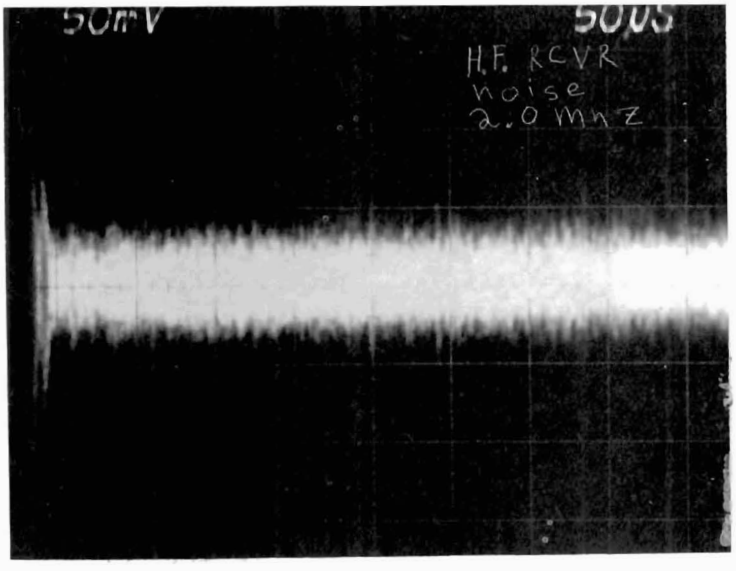

Fig. 41 Operating characteristics of the high frequency EMAT circuits. (a) Transmitter current (10 amp/div, 1 μsec/div). (b) Receiver noise (50 mV/div, 50 μsec/div).

(a)

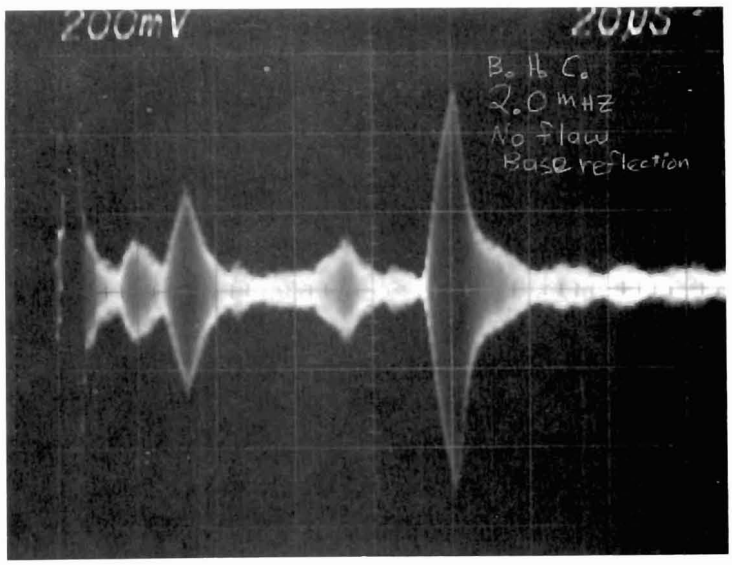

(b)

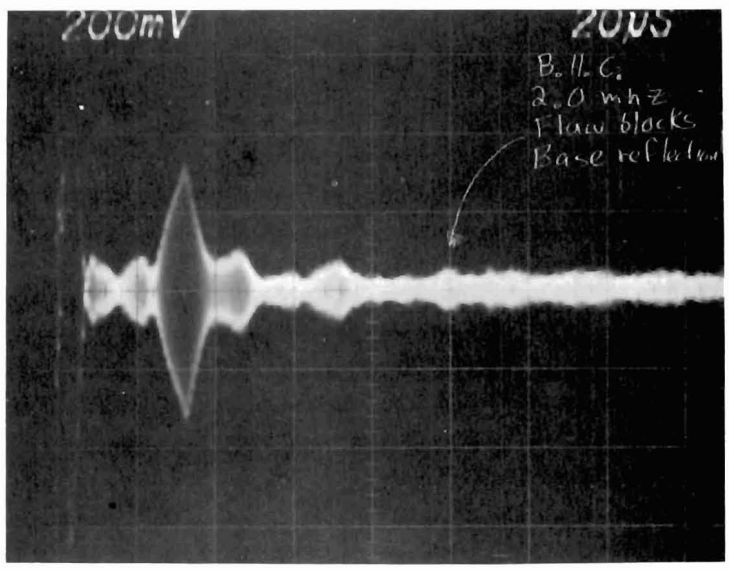

Fig. 42 High frequency, zero degree EMAT signals (a) in an unflawed rail, and (b) signal from EMAT over a bolt hole. (Magnet lift-off ¼", EMAT lift-off 0.03")

(a)

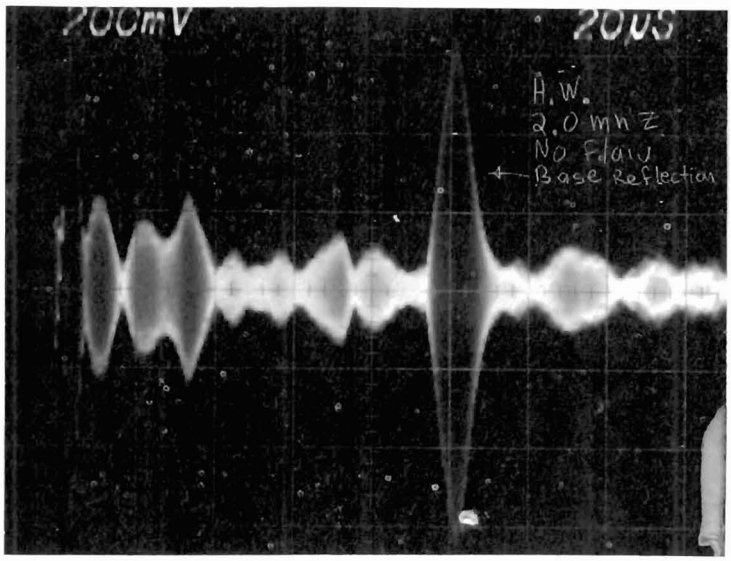

(b)

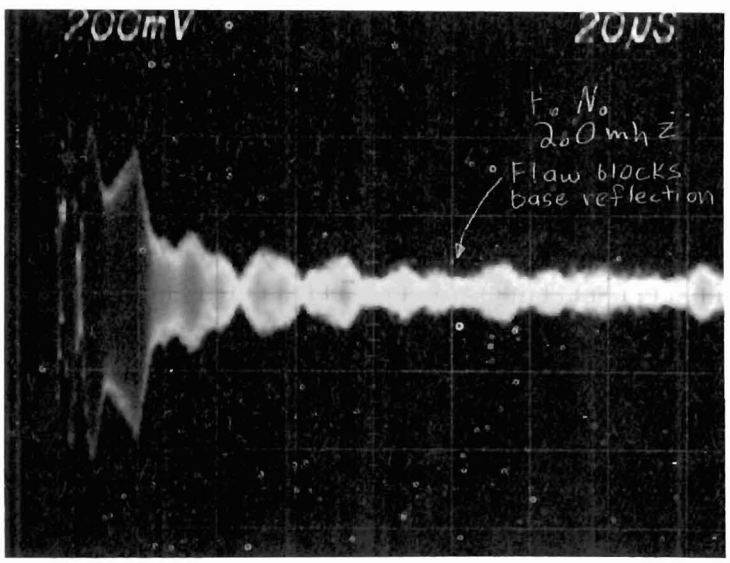

Fig. 43 Disappearance of the base reflection caused by a head and web separation. Note the change in character of the reflection from the bottom of the rail head (at 65 μsec).

(a)

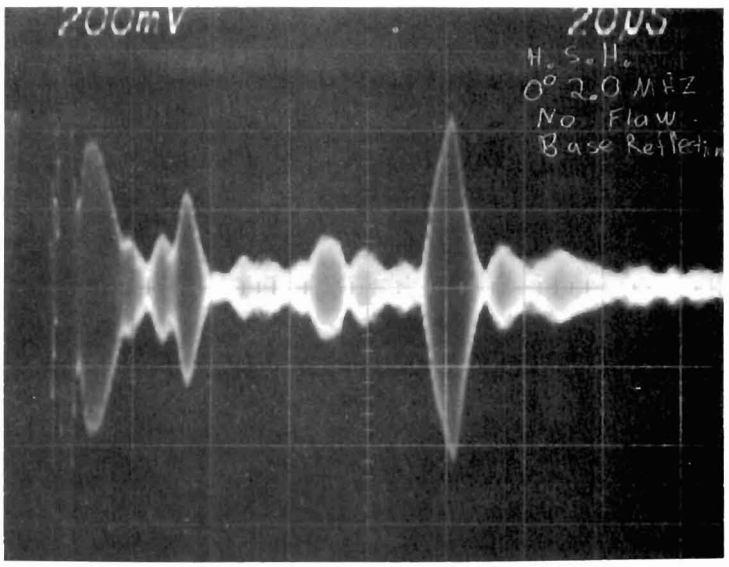

(b)

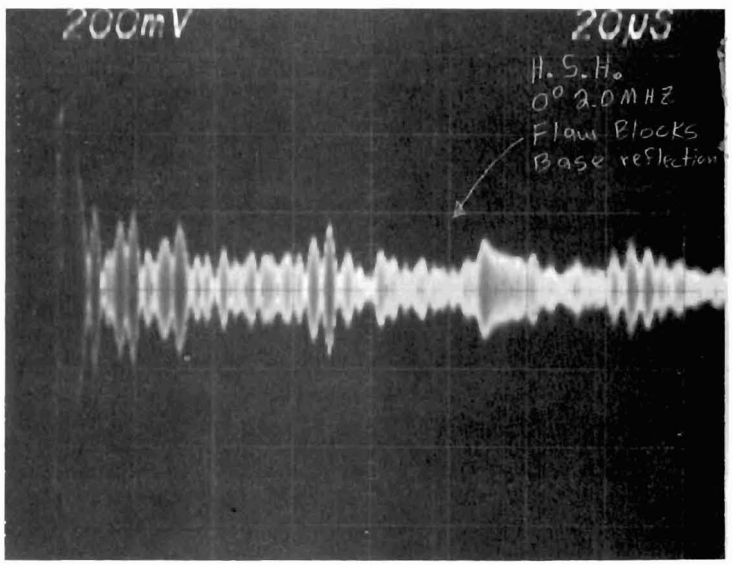

Fig. 44 Disappearance of the base reflection and the elimination of the reflection from the bottom of the rail head produced by a horizontal split head

as is demonstrated in Figs. 43 and 44. It appears possible to distinguish between these particular types of defects on the basis of the changes in the reflection signal from the bottom of the rail head.

Although the vertical split head defect would not appear to be detectable by this 0 degree acoustic wave, because the wave could easily pass around the crack, experiments on rail No. 310 showed that this type of flaw had a dramatic effect on the reflection from the base. Figure 45 (a) shows the oscilloscope display observed on rail No. 310 at a location away from any defects. When placed over the vertical split head region, the base reflection became neglectably small [shown in Fig. 45 (b)]. The observation of such a dramatic scattering of the acoustic signal by a vertical split head may occur because the defect is not truly vertical, and because it certainly has rough faces. Furthermore, the direction of polarization of the shear waves generated by the EMAT used to produce the effect shown in Fig. 45 was perpendicular to the plane of the split, and hence may exhibit a stronger coupling to the flaw than a shear wave polarized parallel to the plane of the split.

An important advantage of the bulk wave EMAT used here is that it is much less sensitive to lift-off than the meander coil EMATs, even of lower frequencies. The lift-off dependence of the 0 degree EMAT used to obtain the data given in Figs. 42 through 45 is shown in Fig. 46. Lift-off distances of greater than 0.06 inches yield adequate signal strength and reasonably good performance up to ¼" is possible. Hence, EMATs with high frequency capabilities (capable of detecting small rail flaws) can be operated at lift-off distances compatible with current field rail inspection techniques.

(a)

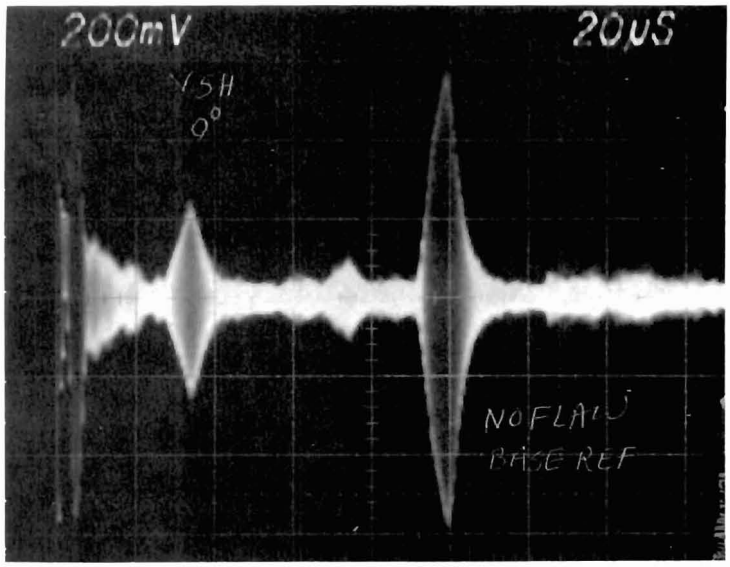

(b)

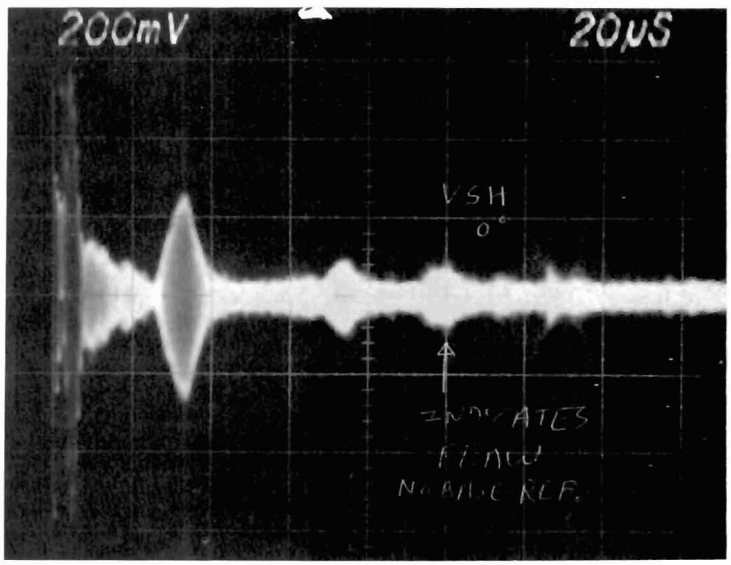

Fig. 45 Appearance of the oscilloscope display: (a) in a flaw-free section of rail No. 310 and (b) over a vertical split head defect. (Magnet lift-off = ¼", EMAT lift-off = 0.03")

Fig. 46 Dependence of the high frequency, 0 degree bulk shear wave transducer.

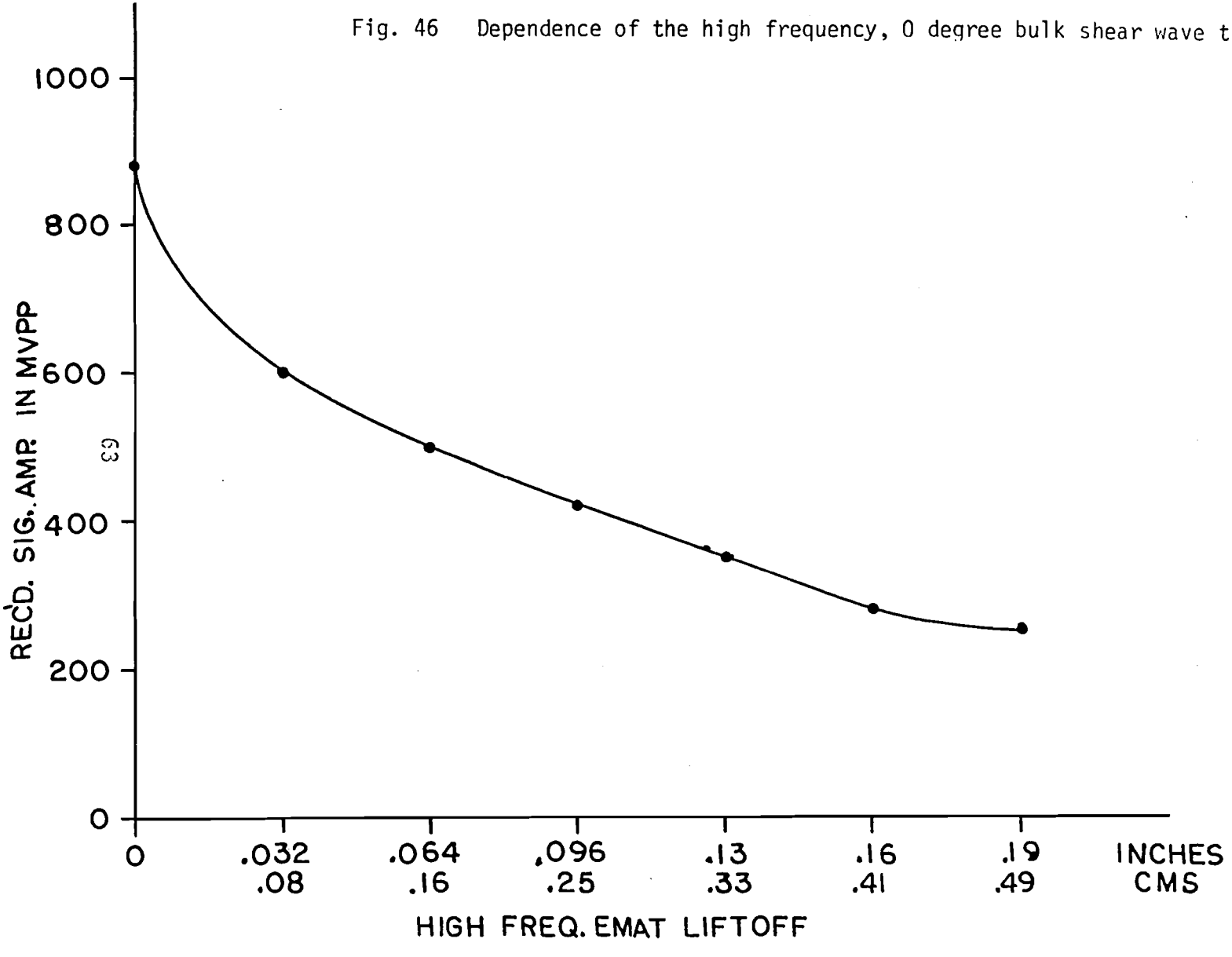

V. CONCLUSIONS

The objective of this first phase effort was to demonstrate the feasibility of applying EMATs to the ultrasonic inspection of rails. Specific EMAT designs and detection schemes were investigated to determine the sensitivity of the inspection process for flaws in a rail when restricted to operate only on the head of the rail with lift-off gaps compatable with field operation. Table 4, lists the defects which were considered in this program along with the types of EMATs that produced optimum detection sensitivity. An X in the column signifies that the EMAT labeled in the column was able to detect the defect listed. A — indicates that detection was marginal while an O indicates that no detection was possible. A Z indicates an anticipated but not determined result. Examination of this table shows that all the defects supplied could be detected by at least one of the EMATs used.

TABLE 4

Results of the Overall Program

Types of "Defects" Investigated	EMAT Design Low Freq.	Med. Freq.	High Freq.
A. Transverse Fissure	X	O	—
B. Compound Fissure	Z	O	—
C. Horizontal Split Head	—	O	X
D. Vertical Split Head	O	O	X
E. Head and Web Separation	O	—	X
F. Bolt Hole Crack	O	X	X
G. Engine Burn Fracture	X	O	O
H. Head Inclusions	X	O	—

Types of "Conditions" Investigated	EMAT Design Low Freq.	Med. Freq.	High Freq.
A. Engine Burn	Z	O	O
B. Weld Repair	X	O	O
C. Surface Shelling	X	O	O
D. Crushed Head	X	O	—

TABLE 5

List of the flaw type present in the rails provided by Sperry Rail Service and the amplitude of the signals produced by these flaws in terms of db relative to electronic noise.

Types of Defects	Approx. Size	Sensitivity
A. Transverse Fissure	15% of the Cross Section of the Head	App. 35 db
B. Compound Fissure	Specimen Not Available	--------
C. Horizontal Split Head	7" long (width unknown)	App. 25 db
D. Vertical Split Head	24" long (width unknown)	App. 25 db
E. Head and Web Separation	8" long (width unknown)	App. 25 db
F. Bolt Hole Crack	2" long (width unknown)	High Freq. 25 db Mid. Freq. 40 db
G. Engine Burn	Specimen Not Available	--------
H. Engine Burn Fracture	15% of the Cross Section of the Head	Flaw close to the end
I. Head Inclusions	15%	App. 35 db
J. Weld Repair	4" long	Flaw close to the end
K. Surface Shelling	4" long (depth unknown)	App. 35 db
L. Crushed Head	4" long	Flaw mixed with horizontal splithead

Table 5, is more quantitative in that it lists the size of the flaw used in the test and the number of db above the electronic noise that the defect signal produced. It must be noted that the acoustic noise, i.e., random echoes arriving at various times was usually 6 to 10 db higher than the electronic noise and actually sets the lower limit to which flaw signals can be detected.

The acoustic noise that limits the minimum size of flaw that can be detected with the EMAT system is the same noise that sets the lower bound to the capability of the currently used piezoelectric systems. This is significant, since the EMAT system is sensitive enough to see the same acoustic noise floor as the piezoelectric transducers, it can be concluded that the EMAT system is as sensitive as is needed to find the range of flaws of current interest in rail inspection. It remains to be seen if this sensitivity can be obtained when the EMAT is moving rapidly over the rail and the minimum lift-off distances can be maintained in practice.

It was shown that satisfactory operation of all three EMAT types can be expected using lift-off gaps of 1/16 inch, which are probably quite tolerable. Other coil design concepts or major improvements in the magnetic field or transmitted power would have to be introduced if lift-off distances were to be increased substantially.

Additional effort is required to improve the total system. Angle beam transducers operating at 60 to 80 degrees relative to the head normal should be investigated to determine their effectiveness at detecting internal transverse flaws. Also 30 to 40 degree angle beam transducers which excite narrower beams of sound should be designed so that only one bolt hole is illuminated at a time and the interference phenomenon need not be used to recognize a crack free bolt hole. A concentration of effort on the most promising EMAT coil designs and frequencies of operation as well as the development of more efficient electromagnets would improve the signal amplitudes and improve detection sensitivity.

In conclusion, this effort has clearly identified the key operating parameters of future EMAT rail inspection systems: 1) Configuration - compared pulse-echo, pitch-catch, and base reflection, 2) Frequency - compared low, mid and high frequency, 3) Angle of inspection - compared 90 (surface), 45° angle and 0°, 4) magnet and EMAT lift-off - at various frequencies, and 5) Proposed novel detection methods for the most critical defect classes, such as bolt hole cracks.

Based on the success of the three frequency EMATs scheme investigated in this program it appears feasible to design an EMAT system to directly replace the 0, 37, and 70 degree piezoelectric transducers now being used on inspection cars in the field and achieve equal or better sensitivity to the range of critical flaws that must be located by inservice rail inspection. This would lead to a much more rapid field inspection approach and be more economical to implement.

VI. ACKNOWLEDGEMENTS

The authors wish to thank the staff of the Sperry Rail Service in Danbury, Connecticut for their efforts in supplying the samples of flawed rails and their cooperation in discussing the various techniques of inspecting rails. Mr. P. Van Hemert and Mr. B. Hendricks deserve special thanks for their critical comments on the strengths and weaknesses of the EMAT and piezoelectric methods as well as for their skill at locating and sizing the defects in the rail samples using portable ultrasonic instruments in Albuquerque.

Several members of the staff of the Albuquerque Development Laboratory also deserve special recognition for their patience and extra efforts in behalf of the program. The many mechanical devices required could not have been made without the help of Mr. Leigh Burns and Mr. Chuck Swanson.

VII. REFERENCES

1. R. B. Thompson, "Electromagnetic Noncontact Transducers," Ultrasonics Symp. Proc. (IEEE, N.Y., 1973), p. 385.

2. R. B. Thompson, "Noncontact Transducers," Ultrasonic Symp. Proc. (IEEE, Phoenix, 1977), p. 74.

APPENDIX A - SAFETY STANDARDS --- TERMINOLOGY & DEFINITIONS

The following is a brief description of different types of rail problems, some of which were investigated during this program. The definitions used are those given in the publication "Track Safety Standards"--Federal Railroad Administration, Office of Safety, March, 1975.

Rail flaws are classed into two general catagories: 1) Defects - which are considered to be serious must have remedial action taken or the rail containing the defect replaced and 2) Conditions - which are less serious but must have some action taken and be reinspected at intervals not more than every 6 months. Defects include the following: transverse fissure, compound fissure, detail fracture, engine burn fracture, defective weld, horizontal and vertical split head, head and web separation, and bolt hole crack and broken base. Conditions include the following: surface shelling, engine burn, crushed head and weld repair.

More detailed description of the defects and conditions are given below. These definitions are largely exerpted from the Rail Safety Standards.

"Defects"

(1) "Transverse Fissure" means a progressive crosswise fracture starting from a crystalline center or nucleus inside the head from which it spreads outward as a smooth, bright, or dark, round or oval surface substantially at a right angle to the length of the rail. The distinguishing feature of a transverse fissure from other types of fractures or defects are the crystalline center or nucleus and the nearly smooth surface of the development which surrounds it.

(2) "Compound Fissure" means a progressive fracture originating in a horizontal split head which turns up or down in the head of the rail as a smooth, bright or dark surface progressing until substantially at a right angle to the length of the rail. Compound fissures require examination of both faces of the fracture to locate the horizontal split head from which they originate.

(3) "Detail Fracture" means a progressive fracture originating at or near the surface of the rail head. These fractures should not be confused with transverse fissures, compound fissures, or other defects which have internal orgins. Detail fractures may arise from shelly spots, head checks, or flaking.

(4) "Engine Burn Fracture" means a progressive fracture originating in spots where driving wheels have slipped on top of the rail head. In developing downward they frequently resemble the compound or even transverse fissure with which they should not be confused or classified.

(5) "Defective Weld" also known as "Head Inclusion" means a progressive transverse separation within an area where two rails have been joined by welding or a rupture at a weld where improper fusion has occured. Defective welds are caused by inclusions, improper fusion during welding, or surface cracks developed from the heat of welding.

(6) "Horizontal Split Head" means a horizontal progressive defect originating inside of the rail head, usually one-quarter inch or more below the running surface and progressing horizontally in all directions, and generally accompanied by a flat spot on the running surface. The defect appears as a crack lengthwise of the rail when it reaches the side of the rail head.

(7) "Vertical Split Head" means a vertical split through or near the middle of the head, and extending into or through it. A crack or rust streak may show under the head close to the web or pieces may be split off the side of the head.

(8) "Head and Web Separation" means a progressive fracture longitudinally separating the head and web of the rail at the fillet under the head. Acid action from some fillers used at highway crossings may start corrosion fatigue where the rail head joins the web. Gravel at crossing, excessive speed on curves, or improper canting of the rail can cause eccentric loading of the rail head. Fatigue then appears as "rail strain", or a creped and wrinkled fillet under the head.

(9) "Bolt Hole Crack" means a progressive fracture which originates at a bolt hole and progresses away from the hole usually at an angle or along a path other than a perpendicular or longitudinal line. A bolt hole crack is usually the result of unusual stresses along the edge of the hole from the bolt itself. These stresses may be caused by pumping or swinging joints, improper drilling, excessively work joint bars, or abnormal rail end impacts from rolling stock. Focal points of bolt hole cracks may be at a stress contact point between the rail and the bolt or at a burr on the edge of the hole left by the drilling operation.

"Conditions"

(1) "Surface Shelling" also called "Shelly Spots" means a condition where a thin (usually three-eights inch in depth or less) shell-like

pieces of surface metal becomes separated from the parent metal in the railhead, generally at the gage corner. It may be evidenced by a black spot appearing on the railhead over the zone of separation or a piece of metal breaking out completely, leaving a shallow cavity in the railhead. In the case of a small shell there may be no surface evidence, the existence of the shell being apparent only after the rail is broken or sectioned.

(2) "Engine Burn" also known as "Burned Rail" is a rail that has been scarred on the running surface by the friction of slipping locomotive drivers. It is caused by intense friction heating from slipping drivers, which overheats and displaces tread metal on the running surface.

(3) "Crushed Head" is a flattening of several inches of the rail head, usually accompanied by a crushing down of the metal but with no signs of cracking under the head. The origin of crushed head is usually a soft spot in the steel of the head, which gives way under heavy wheel loads.

(4) "Weld Repair" small surface defects like engine burn and shelling are ground out and welded to obtain the original shape of the rail.